



HAL
open science

Comparative morphology of snake (Squamata) endocasts: evidence of phylogenetic and ecological signals

Rémi Allemand, Renaud Boistel, Gheylen Daghfous, Zoé Blanchet, Raphael
Cornette, Nathalie Bardet, Peggy Vincent, Alexandra Houssaye

► To cite this version:

Rémi Allemand, Renaud Boistel, Gheylen Daghfous, Zoé Blanchet, Raphael Cornette, et al.. Comparative morphology of snake (Squamata) endocasts: evidence of phylogenetic and ecological signals. *Journal of Anatomy*, 2017, 231 (6), pp.849 - 868. 10.1111/joa.12692 . hal-01681248

HAL Id: hal-01681248

<https://hal.sorbonne-universite.fr/hal-01681248>

Submitted on 1 Feb 2018

HAL is a multi-disciplinary open access archive for the deposit and dissemination of scientific research documents, whether they are published or not. The documents may come from teaching and research institutions in France or abroad, or from public or private research centers.

L'archive ouverte pluridisciplinaire **HAL**, est destinée au dépôt et à la diffusion de documents scientifiques de niveau recherche, publiés ou non, émanant des établissements d'enseignement et de recherche français ou étrangers, des laboratoires publics ou privés.

1 **Comparative morphology of snake (Squamata) endocasts: evidence of phylogenetic and**
2 **ecological signals**

3

4 **Rémi Allemand^{1,2,*}, Renaud Boistel³, Gheylen Daghfous⁴, Zoé Blanchet², Raphaël**
5 **Cornette⁵, Nathalie Bardet¹, Peggy Vincent¹, Alexandra Houssaye²**

6

7 ¹Centre de Recherches sur la Paléobiodiversité et les Paléoenvironnements, CR2P - UMR 7207
8 - CNRS, MNHN, UPMC, Muséum National d'Histoire Naturelle, Sorbonne Universités, 57 rue
9 Cuvier, CP38, F-75005, Paris, France

10 ²UMR 7179 – CNRS / Muséum National d'Histoire Naturelle, Département Adaptations du
11 Vivant, 57 rue Cuvier, CP55, F-75005, Paris, France

12 ³IPHEP-UMR CNRS 6046, UFR SFA, Université de Poitiers, 40 avenue du Recteur Pineau, F-
13 86022, Poitiers, France

14 ⁴Groupe de Recherche sur le Système Nerveux Central, Département de Neurosciences,
15 Université de Montréal, Montréal, Québec, Canada

16 ⁵Institut de Systématique, Evolution, Biodiversité, ISYEB – UMR 7205 – CNRS, MNHN,
17 UPMC, EPHE, Muséum National d'Histoire Naturelle, Sorbonne Universités, 57 rue Cuvier,
18 CP50, F-75005, Paris, France

19

20

21

22

23

24

25 * *Corresponding author: remi.allemand@edu.mnhn.fr*

26 **Abstract**

27 Brain endocasts obtained from computed tomography are now widely used in the field of
28 comparative neuroanatomy. They provide an overview of the morphology of the brain and
29 associated tissues located in the cranial cavity. Through anatomical comparisons between
30 species, insights on the senses, the behavior, and the lifestyle can be gained. Although there
31 are many studies dealing with mammal and bird endocasts, those performed on the brain
32 endocasts of squamates are comparatively rare, thus limiting our understanding of their
33 morphological variability and interpretations. Here, we provide the first comparative study of
34 snake brain endocasts in order to bring new information about the morphology of these
35 structures. Additionally, we test if the snake brain endocast encompasses a phylogenetic
36 and/or an ecological signal. For this purpose, the digital endocasts of 45 snake specimens,
37 including a wide diversity in terms of phylogeny and ecology, were digitized using computed
38 tomography, and compared both qualitatively and quantitatively. Snake endocasts exhibit a
39 great variability. The different methods performed from descriptive characters, linear
40 measurements and the outline curves provided complementary information. All these methods
41 have shown that the shape of the snake brain endocast contains, as in mammals and birds, a
42 phylogenetic signal but also an ecological one. Although phylogenetically-related taxa share
43 several similarities between each other, the brain endocast morphology reflects some notable
44 ecological trends: e.g., 1) fossorial species possess both reduced optic tectum and pituitary
45 gland; 2) both fossorial and marine species have cerebral hemispheres poorly developed
46 laterally; 3) cerebral hemispheres and optic tectum are more developed in arboreal and
47 terrestrial species.

48 **Key words:** computed tomography, brain endocast, snakes, morphometrics, ecological signal,
49 squamates, sensory information.

50

51 **Introduction**

52 Computed Tomography (CT) allows the reconstruction of high-quality 3D models of
53 both hard and soft tissues that can be used for different purposes, such as anatomical and
54 biomechanical studies. It thus constitutes an important exploratory tool in biology and opens a
55 range of new possible investigations (e.g., Boistel et al., 2011a; Carril et al., 2015).

56 Computed tomography is now widely used to visualize the endocranial space with the
57 construction of digital endocasts that may reflect the morphology of the brain and associated
58 tissues (e.g., Anderson et al., 2000; Macrini et al., 2007; Olori, 2010; Bienvenu et al., 2011;
59 Smith & Clarke, 2012; Racicot & Colbert, 2013; Ahrens, 2014; Carril et al., 2015; Corfield et
60 al., 2015; Danilo et al., 2015; Gonzales et al., 2015, Kawabe et al., 2015), the inner ear (e.g.,
61 Chapla et al., 2007; Georgi & Sipla, 2008; Walsh et al., 2009; Ekdale, 2010, 2011, 2013;
62 Willis et al., 2013), the vascular system (e.g., Porter & Witmer, 2015), the cranial nerves (e.g.,
63 George & Holliday, 2013), and pneumatic sinuses (e.g., Bona et al., 2013). Endocasts are
64 generated at the interface between the skeleton (typically bone or cartilage) and the soft
65 tissues (or fluid) lying immediately near it (Balanoff et al., 2015). In the cranial cavity, the
66 soft tissue forming the interface with the surrounding skeleton is not the brain but the
67 superficial surface of the dural meninges, blood vessels and vasculature enveloping the brain
68 (Walsh & Knoll, 2011). Thus, brain endocasts provide only an overview of the external
69 morphology of the brain itself. They may reflect the relative size of the different regions of
70 the brain and could provide some information about sensory abilities, as well as about the
71 behavior and ecology of the species (Walsh & Knoll, 2011).

72 The degree to which the brain endocast reflects the morphology of the brain depends
73 on the degree to which the brain fills the cranial cavity. This factor can vary widely between
74 lineages (e.g., Jerison, 1973; Hopson, 1979; Witmer et al., 2008; George & Holliday, 2013)
75 and over ontogeny (e.g., Macrini et al., 2007; Hurlburt et al., 2013). From different age

76 classes, the brain of the marsupial *Monodelphis domestica* fills between 67.8 and 86.6% of the
77 endocranial volume (Macrini et al., 2007), whereas that of the smallest alligators occupies
78 about 68% of the endocranial space, and about 32% in the largest alligators (Hurlburt et al.,
79 2013). Mammals and birds, which are generally considered as highly encephalized taxa (large
80 brains relative to body size, Balanoff et al., 2015), tend to have brains that nearly fill the
81 cranial cavity, resulting in a strong correlation between the volume and morphology of the
82 brain endocast and those of the brain (Balanoff et al., 2015). Thus, similarly as the brain
83 morphology that may reflect the influence of ecological, behavioral and/or phylogenetic
84 factors (e.g. Lefebvre et al., 2004; Walsh & Milner, 2011), the brain endocast of these taxa
85 tends to have both a phylogenetic and ecologic signals (Lyras & Van Der Geer, 2003; Macrini
86 et al., 2007; Carril et al., 2015; Corfield et al., 2015). Additionally, there is an increasing
87 number of studies performed from brain endocasts of mammals and birds. These studies are
88 generally performed to understand the relation between the mass of the brain and the volume
89 of the cast, but also to consider the intraspecific variability, reflecting either ontogenetic
90 variation, sexual dimorphism, or both (e.g., Macrini et al. 2007; Bienvenu et al., 2011;
91 Kawabe et al., 2015), or finally focusing on the interspecific variability (e.g., Kawabe et al.,
92 2013).

93 Among vertebrates other than mammals and birds, it is generally admitted that the
94 brain does not entirely fill the cranial cavity (Balanoff et al., 2015). A commonly cited
95 estimate considers that the brain occupies only 50% of the endocranial space (Hopson, 1979).
96 However, this ratio is only based on the observation of one *Sphenodon* and one *Iguana* brain
97 specimens (Hurlburt et al., 2013), and is probably far from representing a general pattern in
98 non-endotherms. For example, it has been shown that the brain almost entirely fills the
99 endocranial space in some extant chondrichthyans and teleosts (Northcutt, 2002; Balanoff et
100 al., 2015). Within Squamata (lizards, snakes and amphisbaenians), a wide range of brain

101 versus endocranial cavity proportions were found (Kim & Evans, 2014). The lowest brain–
102 endocranial volume ratio is found in *Gecko gecko* (0.35), whereas the false monitor lizard
103 *Callopietes maculatus* exhibits a brain that nearly fills the endocranial cavity (0.97).
104 Moreover, snakes and amphisbaenians are known to have a brain that fills most of the
105 endocranial space (Starck, 1979; Nieuwenhuys et al., 1998), with a very narrow space
106 between the brain and the cranial wall. The brain may thus fill the intracranial cavity in some
107 squamates, indicating that brain endocasts within these species may reflect the external
108 morphology of the brain with a certain degree of accuracy.

109 Computed tomography (i.e., magnetic resonance imaging (MRI) and X-ray absorption,
110 as well as X-ray phase-contrast imaging techniques) has already been used on skulls of
111 squamates for different purposes, such as the study of the brain (e.g., Anderson et al., 2000),
112 the ear (e.g., Walsh et al., 2009; Boistel et al., 2011b; Christensen et al., 2012; Yi & Norell,
113 2015), and the skull morphology (e.g., Rowe et al., 1999; Bever et al., 2005; Rieppel &
114 Maisano, 2007; Comeaux et al., 2010), the vascular patterns (e.g., Porter and Witmer, 2015),
115 and the lacrimal system (e.g., Souza et al., 2015). But to date only a single study has focused
116 on the brain endocast (Olori, 2010). In her study, Olori reconstructed and described the
117 endocast of the burrowing snake *Uropeltis woodmasoni* and thus provided the first description
118 of a snake brain endocast. However, as no comparative data are available within squamates,
119 the results obtained cannot be discussed in detail. To date, there are several studies published
120 about the brain itself or the central nervous system of squamates (e.g., Senn, 1966; Senn &
121 Northcutt, 1973; Hoogland, 1982; Smeets et al., 1986; Martinez-Garcia et al., 1991; Reperant
122 et al., 1992; Lanuza & Halpern, 1997; Nieuwenhuys et al., 1998; Atobe et al., 2004; Butler &
123 Hodos, 2005; Powell & Leal, 2014) but the exact relationship between brain endocasts and
124 brain morphology remains currently untested for squamates. In addition, data about the brain
125 endocast morphology in this clade are insufficient to fully interpret this structure.

126 The present contribution proposes the first brain endocast comparative study in
127 squamates. It will focus on snakes that are of particular interest since they show a great
128 diversity in morphology, and occupy a wide range of ecologies with e.g., fossorial, aquatic,
129 and arboreal species (e.g., Heatwole, 1999; Greene et al., 2000). Here, we propose to provide
130 a quantitative anatomical description of the brain endocast of a wide sample of snake species
131 using different morphometric approaches in order to: 1) bring new information about this
132 structure, its general traits within snakes and the variation occurring; 2) test if, as in mammals
133 and birds, the brain endocast of snakes reflects a phylogenetic and/or ecologic signal.

134

135 **Material and Methods**

136 **Material**

137 The material consists of the skull of 45 snake specimens (38 genera and 43 species;
138 see Table 1); illustrating the diversity of snakes in both phylogenetic and ecological (i.e.,
139 habitat) perspectives (see Fig. 1). The dataset is divided into six fossorial, seven arboreal,
140 thirteen terrestrial, nine semi-aquatic and ten marine species (Heatwole, 1999; Houssaye et
141 al., 2013; Anthony Herrel, pers. com.). The semi-aquatic group encompasses species that
142 spend most of their time in freshwater without contact with the sea. Three specimens of a
143 single species, *Python regius*, were analyzed in order to evaluate the intraspecific variation.

144

145 **Data acquisition**

146 Microtomography was performed in order to non-destructively digitize the brain
147 endocast of the specimens. The skull of the specimens studied were scanned: (1) at the
148 University of Poitiers (France), Institut de Chimie des Milieux et Matériaux of Poitiers
149 (IC2MP, Poitiers, France) using a X8050-16 Viscom model (resolution between 16.7 and 32.3
150 μm ; reconstructions performed using Feldkamp algorithm with DigiCT software, version 1.15

151 [Digisens SA, France]); and (2) at the European Synchrotron Radiation Facility (ESRF,
152 Grenoble, France) using third generation synchrotron microtomography on beamlines ID 19
153 and BM5 (resolution between 5.0 and 14.9 μm ; reconstructions performed using filtered back-
154 projection algorithm with the ESRF PyHST software).

155 Image segmentation and visualization were performed using VGStudioMax 2.2
156 (Volume Graphics Inc., Heidelberg, Germany) at the Palaeontology Imaging Unit of the
157 MNHN/UMR 7207 CR2P and Avizo 7.0 (VSG, Burlington MA, USA) at the UMR 7179
158 MECADEV. The segmentation tools of these software packages were used to select the
159 endocranial space of the specimens thereby allowing separation of the skull from the
160 endocranial space, and to reconstruct the brain endocast.

161

162 **Institutional abbreviations**

163 **IC2MP**, Institut de Chimie des Milieux et Matériaux, Poitiers, France; **ESRF**, European
164 Synchrotron Radiation Facility, Grenoble, France ; **MCZ**, Museum for Comparative Zoology,
165 Harvard University, U. S. A.; **MNHN**, Muséum National d'Histoire Naturelle, Paris, France ;
166 **ZRC**, Zoological Reference Collections, National University of Singapore.

167

168 **Measurements**

169 For each specimen, 21 measurements were defined and taken to illustrate the whole
170 3D shape, volume and surface of the brain endocast (see Fig. 2B). All the measurements made
171 on the brain endocast were measured point-to-point and obtained with the digital caliper of
172 VGStudioMax 2.2 and the measuring tool of Avizo 7.0, both with accuracy of 0.01mm (see
173 Supporting information S1 & S2). The print of the sutures between the different skull bones
174 visible on the brain endocast surface were used to define homologous distances. The
175 following list introduces the measurements taken on the brain endocast. The different parts of

176 the brain endocast are named with the same terms as those used for the brain itself (see Fig.
177 2A), following Butler & Hodos (2005); however the terms used here do not have a
178 neurological significance and are not related to neural structures.

179 (a) *Length of the brain endocast (LE)*: distance between the anteriormost part of the
180 olfactory bulbs still entirely surrounded by the frontal bone and the tip of the suture left by the
181 contact of the supraoccipital with the two exoccipitals on the dorsal surface of the brain
182 endocast;

183 (b) *Length of the olfactory bulbs (LOB)*: distance between the anteriormost part of the
184 olfactory peduncles still entirely surrounded by the frontal bone and the fronto-parietal suture;

185 (c) *Length of the groove between the olfactory bulbs (LG)*: distance between the
186 anteriormost end of the groove between the olfactory peduncles and the fronto-parietal suture;

187 (d) *Height of the main olfactory bulb (HOB)*: at the level of the anteriormost part of
188 the main olfactory bulb still entirely surrounded by the frontal bone;

189 (e) *Height of the olfactory peduncle (HOP)*: at the level of the fronto-parietal suture;

190 (f) *Width of the olfactory peduncles (WOP)*: at the level of the fronto-parietal suture;

191 (g) *Length of the fissura interhemispherica (LFI)*: distance between the fronto-parietal
192 suture and the virtual limit made by the groove between the cerebral hemispheres and the
193 optic tectum;

194 (h) *Maximal width of the cerebral hemispheres (WCH)*;

195 (i) *Lateral expansion of the cerebral hemispheres (LCH)*: distance between the
196 fronto-parietal suture and the posterior end of the lateral margin of the cerebral hemispheres;

197 (j) *Maximal height of the cerebral hemispheres (HCH)*;

198 (k) *Maximal width of the optic tectum (WOR)*;

199 (l) *Length of the optic tectum (LOR)*: distance between the virtual limit made by the
200 groove separating the cerebral hemispheres of the optic tectum (see Fig. 2B) and the tip of the
201 V-shaped suture between the parietal and the supraoccipital (see Fig. 2A);

202 (m) *Height of the optic tectum (HOR)*: distance between the dorsal surface of the optic
203 tectum and the triple point formed by the suture between the parietal, prootic and
204 basisphenoid (see Fig. 2A);

205 (n) *Length of the pituitary gland (LP)*: distance between the fronto-parietal suture and
206 the most posterior point of the pituitary bulb;

207 (o) *Height of the pituitary gland (HP)*: distance between the most ventral point of the
208 pituitary gland and the triple point formed by the sutures between the parietal, prootic and
209 basisphenoid;

210 (p) *Width of the inner ear region (WIE)*: distance between the two triple points
211 formed by the sutures of the supraoccipital, prootic and exoccipital;

212 (q) *Dorsal width of the posterior end of the brain endocast (DWPE)*: distance taken at
213 the level of the suture between the supraoccipital and the two exoccipitals seen on the dorsal
214 surface of the brain endocast;

215 (r) *Length of the posterior part of the brain endocast (LPE)*: distance between the tip
216 of the V-shaped suture between the parietal and the supraoccipital, and the tip of the V-shaped
217 suture between the supraoccipital and the two exoccipitals;

218 (s) *Height of the posterior part of the brain endocast (HPE)*: distance between the
219 maximum of concavity of the inner ear region and the ventral margin of the brain endocast;

220 (t) *Width of the ventral part of the brain endocast (WPE)*: distance between the two
221 triple points formed by the suture between the prootic, basisphenoid and basioccipital on the
222 ventral margin;

223 (u) *Width in the pituitary gland region (WP)*: distance taken on the ventral surface of
224 the brain endocast, between the triple points formed by the sutures between the parietal,
225 prootic and basisphenoid.

226

227 **Quantitative analyses**

228 In order to provide complementary information, three different approaches were used
229 to study the brain endocast variability occurring in snakes.

230

231 *Descriptive character analysis*

232 The differences observed between the various snake brain endocasts were listed and
233 coded (See Supporting information S3: List of the characters and Matrix). We used the coded
234 characters to run a principal coordinate analysis (PCoA) in order to evaluate the distances
235 between the taxa and thus to identify which taxa are similar in brain endocast morphology
236 based on these coded characters: the closest the species, the more similar the brain endocast
237 morphologies.

238

239 *Measure analysis*

240 All data (see Supporting information S1 & S2) were log₁₀-transformed prior to
241 analysis to meet assumptions of normality and homoscedasticity required for parametric
242 analyses. All the analyses were performed using the statistic software R (R Development Core
243 Team, 2008). To analyze shape components independently from size, the log-shape ratios
244 (Mosimann & James, 1979) were calculated based of the raw log₁₀-transformed linear
245 dimensions of the brain endocast.

246 In order to take into account the biases induced by measurement repeatability, three
247 specimens of *Python regius* showing the lowest shape variation were selected. According to

248 the data published by Aubret et al. (2005), the comparison of their jaw length seems to
249 differentiate a neonate specimen (P1; jaw length = 25.4 mm) from a juvenile (P3; jaw length
250 = 31.4 mm) and an adult (P2; jaw length = 40.3 mm) ones. Ten repetitions were performed for
251 each measure on these three specimens. Then, to quantify and visualize the differences
252 between repetitions, a Principal Component Analysis (PCA) was performed. Shape
253 differences between specimens were much higher than shape differences induced by
254 repetitions (see Supporting information S2).

255 To evaluate the phylogenetic signal in the shape on the brain endocast in snakes, we
256 used a multivariate generalization of the K statistic of Blomberg et al. (2003): the K_{mult}
257 (Adams, 2014). The phylogenetic signal is based on a phylogenetic consensus tree derived
258 from several published phylogenies (Pyron et al., 2011; Hsiang et al., 2015; Lee & Scanlon,
259 2002; Fig. 1). Adams (2014) demonstrated that values of $K_{mult} < 1$ imply that taxa resemble
260 each other phenotypically less than expected under Brownian motion whereas values of
261 $K_{mult} > 1$ imply that close relatives are more similar to one another phenotypically than
262 expected under Brownian motion. A PCA was also performed on the data obtained from the
263 measurements made on the 45 snake specimens; the mean of the 10 measurements taken on
264 each of the *Python regius* specimens was used.

265 To test the relationships between the habitat/ecology and the morphology of the brain
266 endocast, the sampled taxa were classified into five habitat categories (see Fig.1): fossorial,
267 terrestrial, arboreal, semi-aquatic, and marine (Heatwole, 1999; Houssaye et al., 2013; A.
268 Herrel, pers. comm.). We performed a standard and phylogenetic MANOVA, to respectively
269 evaluate whether the brain endocast variability could reflect the ecology, taking or not the
270 phylogenetic relationships into consideration.

271

272 *Outline curve analysis*

273 For each brain endocast, the ventral and lateral views were selected to perform an
274 outline curve analysis using geometric morphometrics (Zelditch et al., 2004). We used 2D
275 sliding semi-landmarks (Gunz & Mitteroecker, 2013) that permit accurate description of
276 homologous anatomical curves devoid of anatomical landmarks. Sliding semi-landmarks are
277 allowed to slide, minimizing the bending energy between each specimen and the mean shape
278 of the data set. This step creates a geometric homology between specimens that permits all
279 classical geometric morphometric analyses. We performed a General Procrustes
280 Superimposition to work on shape (Rohlf, & Slice, 1990) and PCAs for each view.

281 The dorsal view was not used here because of the difficulty to distinguish homologous
282 outline curves on the posterior part of the structure at the level of the inner ear position. In
283 ventral view, the 45 brain endocasts of our dataset were used. In lateral view, we used the
284 posterior crest formed by the inner ear and three homologous points as landmarks to facilitate
285 the placement of the curve semilandmarks. The sutures between the different skull bones
286 visible on the posterior part of the brain endocast surface were used to define homologous
287 points. The first point corresponds to the triple point formed by the sutures between the
288 basioccipital, exoccipital and prootic. The second is the triple point formed by the prootic, the
289 basioccipital and the basisphenoid. The last point represents the most ventral point of the
290 suture between the basioccipital and the basisphenoid. In lateral view, we used 38 specimens
291 because the sutures are not visible and did not allow the placement of the same landmarks on
292 *Aipysurus eidouxii*, *Cerebrus rynchops*, *Corallus hortulanus*, *Dispholidus typus*, *Mimophis*
293 *mahfalensis*, the smallest specimen of *Python regius* and *Uropeltis pulneyensis*.

294

295 **Results**

296 **General description of snake endocast and variability**

297 Here, only a description of the brain endocast will be provided, without considering
298 the cranial nerves or the inner ear (data in Boistel et al., 2011b; Yi & Norell, 2015). The cast
299 of the endocranial space does not only reflect the brain itself: associated tissues (e.g., venous
300 system) are also reconstructed during segmentation and may hide some parts of the brain. The
301 endocast morphology resulting from the segmentation of the endocranial space is described
302 below as a whole. The brain endocast in snakes is surrounded dorsally by the frontal and
303 parietal (anteriorly) and the supraoccipital and exoccipital (posteriorly), laterally by the
304 prootics, and ventrally by the basioccipital and para-basisphenoid. The surface of the brain
305 endocast of snakes is smooth.

306

307 *Telencephalon*

308 The telencephalon includes the olfactory bulbs, the olfactory peduncles and the
309 cerebral hemispheres (see Fig. 2A). The main and accessory olfactory bulbs correspond to the
310 anteriormost structure of the brain endocast (see Fig. 2A); however, from the brain endocast
311 only it is not possible to distinguish one from another. They are attached to the rostral pole of
312 the cerebral hemisphere by short olfactory peduncles. In dorsal view, a groove is visible
313 running between the two olfactory bulbs. Posteriorly, the cerebral hemispheres represent the
314 largest part of the brain endocast and gradually widen laterally. An interhemispheric fissure
315 may be visible on the dorsal surface of the brain endocast, as attested by a groove between the
316 cerebral hemispheres. The length of the interhemispheric fissure and the depth of the groove
317 vary according to taxa.

318 Some taxa may exhibit olfactory bulbs wider than long, giving a short and stout aspect
319 (e.g., width/length aspect ratio superior to one in *Typhlophys squamosus*, see Fig. 4A) in

320 dorsal view, while most taxa have an olfactory structure longer than wide (e.g., width/length
321 aspect ratio inferior to one in *Hierophis viridiflavus*, see Fig. 4B). The lateral margin of this
322 structure may be mediolaterally convex (e.g., *Acrochordus granulatus*, see Fig. 4D), relatively
323 straight (e.g., *Eunectes murinus*, see Fig. 4E) or mediolaterally concave (e.g., *Hierophis*
324 *viridiflavus*, see Fig. 4B) in dorsal view. Most species possess in dorsal view a system
325 composed of two parallel olfactory bulbs and peduncles (e.g., *Eunectes murinus*, see Fig. 4E).
326 Some others show a projection that diverges laterally from the fronto-parietal suture (e.g.,
327 *Homalopsis buccata*, see Fig. 4F), whereas others share the two conditions with parallel
328 olfactory bulbs and peduncles diverging laterally at their anterior end (e.g., *Hierophis*
329 *viridiflavus*, see Fig. 4B). In lateral view, the ventral margin may be ventrodorsally concave
330 (e.g. *Mimophis mahfalensis*, see Fig. 5D), convex (e.g., *Boiga dendrophila*, see Fig. 5B)
331 forming a bulge, or straight (e.g., *Homalopsis buccata*, see Fig. 5C). Some taxa (e.g.,
332 *Typhlophys squamosus*, see Fig. 4A) do not show any separation over the whole length of the
333 olfactory peduncles in dorsal view. Most taxa have olfactory peduncles diverging only at their
334 anterior end (e.g., *Hierophis viridiflavus*, see Fig. 4B). Some species have a large space
335 between the two olfactory structures, separating them along almost their entire length (e.g.,
336 *Acrochordus granulatus*, see Fig. 4D). The width of the olfactory bulbs may vary antero-
337 posteriorly. At the level of the fronto-parietal suture and in dorsal view, some taxa possess a
338 posterior part as wide (e.g., *Eunectes murinus*, see Fig. 4E) or wider (e.g., *Cylindrophis ruffus*,
339 see Fig. 4C) than the anterior end. However, others have olfactory bulbs with an anterior end
340 wider than the posterior part (e.g., *Hierophis viridiflavus*, see Fig. 4B).

341 The relative size of the cerebral hemispheres varies between taxa. A distinction is
342 seen between those that have hemispheres wider than long (e.g., width/length aspect ratio
343 close to 1.4 in *Chrysopelea ornata*, see Fig. 4G) and those that have a structure as long as
344 wide (e.g., width/length aspect ratio close to one in *Typhlophys squamosus*, see Fig. 4A). A

345 few taxa are exceptions with cerebral hemispheres longer than wide (e.g., width/length aspect
346 ratio close to 0.3 in *Cylindrophis ruffus*, see Fig. 4C). The lateral extension in dorsal view
347 generally begins just posterior to the fronto-parietal suture (e.g., *Eunectes murinus*, see Fig.
348 4E) but two taxa (*Cylindrophis ruffus* [Fig. 4C] and *Anilius scytale* [Fig. 4H]) exhibit cerebral
349 hemispheres with an anterior part as wide as the fronto-parietal suture, the lateral extension
350 occurring more posteriorly. In dorsal view, the lateral margin may be rounded (e.g., *Eunectes*
351 *murinus*, see Fig. 4E) or relatively straight (e.g., *Chrysopelea ornata*, see Fig. 4G), providing
352 a square appearance to the cerebral hemispheres. In lateral view, differences occur between
353 taxa with cerebral hemispheres developed only along the horizontal axis (e.g., *Typhlophys*
354 *squamosus*, see Fig. 5A), taxa with cerebral hemispheres developed in the horizontal plane
355 but with a posterior part directed ventrally (e.g., *Homalopsis buccata*, see Fig. 5C) and taxa
356 with a dorso-ventral extension at least as long as the horizontal one (e.g., *Boiga dendrophila*,
357 see Fig. 5B). The limit between the cerebral hemispheres and the optic tectum depends on the
358 lateral extension of the cerebral hemispheres. Species that do not have an important lateral
359 extension (e.g., *Anilius scytale*, see Fig. 4H) do not show a clear delimitation between the
360 optic tectum and the cerebrum, contrary to those that have a groove between the two
361 structures and have laterally extended cerebral hemispheres (e.g., *Chrysopelea ornata*, see
362 Fig. 4G).

363

364 *Diencephalon*

365 The pituitary gland, located ventrally to the cerebral hemispheres, is the only structure
366 of the diencephalon seen on the brain endocast (see Fig. 2A); the pineal gland is not visible. In
367 addition, the external morphology of the brain endocast does not allow the hypothalamus and
368 the hypophysis to be delimited.

369 The pituitary gland may be marked by the presence in lateral view of a small bulge on
370 the ventral surface of the brain endocast (e.g., *Anilius scytale*, see Fig. 5E). But generally the
371 system shows a structure more developed ventrally, displaying (e.g., *Hierophis viridiflavus*,
372 see Fig. 5F) or not (e.g., *Eunectes murinus*, see Fig. 5G) a posterior projection. Among those
373 displaying a posterior projection, a distinction is made between those presenting a tilted
374 system (e.g., *Enhydrina schistosa*, see Fig. 5H) and those having a posterior projection in the
375 horizontal plane (e.g., *Hierophis viridiflavus*, see Fig. 5F). Differences relative to the ventral
376 margin of the posterior projection also occur, between a curved (e.g., *Thamnophis sirtalis*, see
377 Fig. 5J) and a flat (e.g., *Dispholidus typus*, see Fig. 5I) shape.

378

379 *Mesencephalon*

380 The mesencephalon lies posterior to the cerebral hemispheres. The optic tectum forms
381 the roof of the mesencephalon (see Fig. 2A). From the endocast, the distinction between the
382 optic tectum and the tegmentum, which is located more ventrally in the mesencephalon, is not
383 possible. In dorsal view, the mesencephalon is less wide than the cerebral hemispheres.

384 In a few taxa this structure is not distinguishable from the cerebral hemispheres (e.g.,
385 *Typhlophys squamosus*, see Fig. 4A). In some others, the structure is visible in dorsal view
386 only thanks to its decrease in width as compared to the cerebral hemispheres (e.g., *Eunectes*
387 *murinus*, see Fig. 4E), and its surface appears smooth and flattened. However, in other
388 species, the optic tectum exhibits in dorsal view a pair of domes separated by a median sulcus
389 (e.g., *Thamnophis sirtalis*, see Fig. 6A). Some taxa show (in dorsal view) a distinct optic
390 tectum as wide as the rhombencephalon (e.g. *Homalopsis buccata*, see Fig. 4F). The others
391 have an optic tectum wider (e.g., *Chrysopelea ornata*, see Fig. 4G) or narrower (e.g.,
392 *Acrochordus granulatus*, see Fig. 4D) than the ventral margin of the rhombencephalon. In
393 lateral view, most taxa possess a dorsal margin of the optic tectum located at the same height

394 as the cerebral hemispheres (e.g., *Eunectes murinus*, see Fig. 5G), except *Erpeton*
395 *tentaculatum*, in which the margin is located more dorsally (see Fig. 6D).

396

397 *Rhombencephalon*

398 Posterior to the optic tectum, the cerebellum is not visible on the dorsal surface of the
399 brain endocast. According to Aurboonyawat et al. (2008), the dorsal longitudinal vein located
400 on the mid-dorsal surface of the brain endocast must cover it. On the lateral sides of the brain
401 endocast, the large and round impressions indicate the position of the inner ear (see Fig. 2A).
402 The *medulla oblongata* is located ventral to the inner ear region, and represents the ventral
403 margin of the posterior part of the brain endocast.

404 Most species exhibit a rhombencephalon in lateral view with a rounded (e.g., *Boa*
405 *constrictor*, see Fig. 7A) or straight (e.g., *Erpeton tentaculatum*, see Fig. 6D) ventral margin,
406 but in some taxa (e.g., *Crotalus atrox*, see Fig. 7B) the ventral margin is triangular, pointing
407 ventrally. The ventral extension of the *rhombencephalon* may correspond to the most ventral
408 surface of the brain endocast in lateral view (e.g., *Boa constrictor*, see Fig. 7A) or not (e.g.,
409 *Dispholidus typus*, see Fig. 5I).

410

411 **Quantitative analyses**

412 Brain endocasts of snakes show a great variability. This variability is characterized by
413 different relative proportions between the structures visible on the brain endocasts (e.g., size
414 of the optic tectum compared to that of the cerebral hemispheres), giving a wide range of
415 shapes, from stout (e.g., *Typhlophis squamosus*), to elongated and gracile (e.g., *Pelamis*
416 *platurus*) or elongated and wide (e.g., *Boa constrictor*) brain endocasts. Below, this variability
417 is analyzed quantitatively.

418

419 *Descriptive character analysis*

420 The results obtained (Fig. 8) show that 50.3 % of the variance is explained by the two
421 main principal components (29.4 % and 20.9 % respectively). The distribution of the taxa
422 indicates that fossorial and marine snakes are both distinct from those with other ecologies.
423 Among the fossorial species, *Atractaspis irregularis* is quite distinct from two groups: the
424 first one including *Uropeltis pulneyensis*, *Cylindrophis ruffus*, and *Anilius scytale*, and the
425 second one made by *Typhlophis squamosus* and *Rhinotyphlops schlegelii*. *Micrurus*
426 *lemniscatus* and *Acrochordus granulatus*, a terrestrial and a semi-aquatic snakes, respectively,
427 tend toward the brain endocast morphology found in the fossorial taxa. Among the marine
428 species of our dataset, *Enhydrina schistosa* and *Microcephalophis gracilis* are close to each
429 other and distinct from other marine snakes. The terrestrial species show a wide distribution.
430 The isolated position of *M. lemniscatus* was already cited above. *Hierophis gemonensis*,
431 *Hierophis viridiflavus*, and *Thamnophis sirtalis* are close together and located near the two
432 arboreal snakes *Dispholidus typus* and *Chrysopelea ornata*. These species are distinct from
433 *Mimophis mahfalensis*, *Crotalus atrox*, *Agkistrodon contortrix*, *Coronella austriaca* and *Naja*
434 *nivea*, which are close together and possess a brain endocast morphology similar to the
435 arboreal snakes *Boiga dendrophila* and *Dasypeltis* sp. In addition, the three specimens of
436 *Python regius* and *Candoia* sp., are distinct from the other terrestrial taxa with a brain
437 endocast morphology tending towards those found in marine ones. Among the arboreal taxa
438 not cited above, *Corallus hortulanus*, *Boa constrictor* and *Pareas margaritophorus* are close
439 to the semi-aquatic snake *Cantoria violacea*. The distribution of the semi-aquatic species
440 overlaps those of the terrestrial and arboreal snakes. The brain endocast of *Enhydris enhydris*
441 is similar to that of *M. mahfalensis* and distinct from those of *Erpeton tentaculum*, *Fordonia*
442 *leucobalia*, *Homalopsis buccata*, and *Enhydris punctata*, which are grouped together. The two

443 species *Cerberus rynchops* and *Eunectes murinus* are respectively close to *Candoia* sp. and to
444 the three specimens of *P. regius*, and tend towards the marine taxa.

445 The species distribution suggests the existence of phylogenetic and ecological signals.
446 Phylogenetically close species show more similarities than with other species (e.g.,
447 *Typhlophis squamosus* and *Rhinotyphlops schlegelii*). However, an ecological signal is also
448 perceived, meaning that species sharing the same ecology show more brain endocast
449 similarities than species with a different ecology.

450

451 *Measure analysis*

452 Intraspecific variability in *Python regius*

453 The PCA (see Fig. 9) shows that the two main axes explain 93 % of the variance (80
454 % and 13 % respectively). The repeatability test is positive as the ten iterations for each
455 specimen are clearly grouped and the three specimens clearly distinct, indicating that the
456 variability caused by the measurement acquisition is inferior to the variability between the
457 specimens. All variables seem to act on the distribution of the specimens (though the impact
458 of LP (Length of the pituitary bulb) on the second axis appears significantly more important
459 than that of the other variables). The first principal component mostly separates the specimens
460 based on size. The variables principally acting on PCA1 are the height of the olfactory bulbs
461 (HOB), the length of the optic tectum (LOR) and the length of the pituitary gland (LP). The
462 smaller specimen (P1) has the greatest height of the olfactory bulbs, the greatest length of the
463 pituitary bulb, and the smallest length of the optic tectum. The second principal component
464 separates the intermediate specimen (P3) from the two others. The main variable acting along
465 the second axis is still the length of the pituitary gland (LP). The intermediate specimen (P3)
466 shows the smallest height of the olfactory bulb, the greatest length of the optic tectum and an
467 intermediate value for the length of the pituitary gland. Finally, the largest specimen (P2)

468 possesses the greatest length of the pituitary gland, and intermediate values for the height of
469 the olfactory bulb and for the length of the optic tectum.

470

471 Interspecific variability

472 The PCA obtained with all snake specimens (see Fig. 10) shows that 60 % of the
473 variance is explained by the two first axes (44.7% and 15.3% respectively). Fossorial species
474 are clearly distinct from the others, with a great distribution along the first axis, contrary to
475 the snakes with other ecologies, that all display a more limited distribution. The PCA shows
476 some overlap between the snakes with arboreal, terrestrial, semi-aquatic and marine habitats,
477 but a gradation is clearly visible. The arboreal and terrestrial taxa appear distinct (with no
478 overlap) from the marine ones. All variables seem to act on the repartition of the species (see
479 Supporting information S4). However, along the first axis, two variables mostly act on the
480 distribution of the taxa: the width at the optic tectum level (WOR) and the dorsal width of the
481 posterior end of the brain endocast (DWPE). The first axis seems to separate species that have
482 an optic tectum as wide as the posterior end of the brain endocast (e.g., *Typhlophis*
483 *squamosus*) from the ones in which the optic tectum is much wider than the posterior end of
484 the brain endocast (e.g., *Pelamis platurus*). Along the second axis, the width of the olfactory
485 peduncles (WOP) and the width of the cerebral hemispheres (WCH) explain most of the
486 variability. These variables allow to distinguish species presenting a large difference between
487 the width of the olfactory peduncles and the width of the cerebral hemispheres (e.g., *Boa*
488 *constrictor*), from those that have a smaller difference between these two widths (e.g.,
489 *Cylindrophis ruffus*).

490 The MANOVA performed on the data indicates significant differences between brain
491 endocasts depending on ecology (MANOVA: Wilks $\lambda = 0.751$, $F_{2, 22} = 8.75$, $P = 0.013$). The
492 Kmult test indicates that brain endocast shape in snakes exhibits a significant phylogenetic

493 signal ($K_{mult} = 0.814$; $P.value = 0.001$), showing the importance to consider the phylogeny in
494 studies of snake brain endocasts. The phylogenetic MANOVA still indicates significant
495 differences pending on ecology (phylogenetic MANOVA: Wilks $\lambda = 0.0074$, $F_{2, 22} = 81.748$,
496 $P_{phyl} = 0.0087$).

497

498 *Outline curve analysis*

499 The results obtained by the outline curve analyses (Fig. 11 and 12) enable to comment
500 on the shape of snake brain endocasts according to the different ecologies.

501 The first PCA is obtained from the endocast outline curves in ventral view (Fig. 11)
502 and shows that 61.9% of total variance is explained by the two first axes (44.6% and 17.3%
503 respectively). The first axis separates proportionally stout brain endocasts, wide at the level of
504 the olfactory bulbs and of the cerebral hemispheres (blue dotted line, Fig. 11, Axis 1), from
505 longer and narrower endocasts (black dotted line, Fig. 11, Axis 1). Thus, brain endocasts of
506 semi-aquatic, arboreal and terrestrial snakes are mostly wide, whereas the fossorial and
507 marine species have an extended distribution along this first axis, encompassing both wide
508 and narrow endocasts. However, the distribution of marine taxa is mainly concentrated
509 towards narrow endocasts and only two species, *Aipysurus duboisii* and *Aipysurus eydouxii*,
510 move towards wide endocasts. Along the second axis, the shape of the forebrain (olfactory
511 bulbs and cerebral hemispheres) principally drives the distribution. Brain endocasts with wide
512 olfactory bulbs have cerebral hemispheres located more anteriorly (dark dotted line, Fig. 11,
513 Axis 2) than those with thinner olfactory bulbs (blue dotted line, Fig. 11, Axis 2). Semi-
514 aquatic, fossorial and marine species all exhibit a brain endocast with wide olfactory bulbs
515 and anteriorly located cerebral hemispheres, contrary to the arboreal and terrestrial snakes that
516 are distributed all along the axis and thus express the two conditions.

517 The second PCA is obtained from the endocast outline curves in lateral view (Fig. 12)
518 and shows that 65.8% of total variance is explained by the two first axes (48% and 17.8%
519 respectively). The first axis illustrates brain endocasts with well dorsoventrally developed and
520 ventrally oriented olfactory bulbs, and a posterior part characterized by a rounded dorsal
521 surface more developed dorsally than the anterior part (blue dotted line in Fig. 12, Axis 1).
522 These brain endocasts differ from those in which the olfactory bulbs are less developed
523 dorsoventrally and dorsally oriented, and the posterior part presents a flat dorsal surface
524 located at the same level as the anterior part (dark dotted line Fig. 12, Axis 1). The brain
525 endocast of the fossorial species *Rhinotyphlops schlegelii* is well distinct from those of other
526 taxa, with a structure very developed dorsoventrally and the posterior region higher than the
527 anterior one. Arboreal and terrestrial species may show a mix between the two morphologies,
528 with a well dorsoventrally developed brain endocast but a flat posterior region located at the
529 same level as the anterior one. Marine snakes tend to have a flat brain endocast, whereas
530 semi-aquatic and fossorial taxa show a large distribution presenting the two brain endocast
531 morphologies. The second axis separates stout brain endocasts well developed dorsoventrally,
532 with a slight dorsal constriction at the limit between the olfactory bulbs and the cerebral
533 hemispheres (blue dotted line Fig. 12, Axis 2) from longer but less dorsoventrally developed
534 brain endocasts (dark dotted line Fig. 12, Axis 2), with a ventral constriction at the limit
535 between the olfactory bulbs and the cerebral hemispheres. The distribution of the taxa seems
536 to indicate that the two morphologies are variably found in all ecologies. However, the
537 dorsoventrally compressed brain endocast found in both marine (*Pelamis platurus*) and
538 terrestrial (*Candoia* sp.) snakes, differs from the more dorsoventrally developed brain
539 endocasts found in other taxa sharing their ecologies.
540

541 **Discussion**

542 **Phylogenetic signal**

543 We detected a significant phylogenetic signal in the snake brain endocast variability,
544 meaning that it is at least partly constrained by shared ancestry. Indeed, some patterns or main
545 trends in the brain endocast morphology reflect snakes' systematics. The scolecophidian
546 snakes (*R. schlegelii* and *T. squamosus*, see Fig. 1) are the only ones presenting a brain
547 endocast where the optic tectum is not visible (see Fig. 4A). Within the Booidae (see Fig. 1),
548 the surface of the optic roof is smooth (e.g., *Eunectes murinus*, see Fig. 4E), and the pituitary
549 gland is only developed ventrally. The Hydrophiidae (see Fig. 1) have cerebral hemispheres
550 poorly developed laterally (e.g., *Enhydrina schistosa*, see Fig. 5H), contrary to the Colubridae
551 (see Fig. 1) that possess cerebral hemispheres very developed both laterally and ventrally
552 (e.g., *Hierophis viridiflavus*, see Fig. 4B, 5F), as well as an optic roof clearly visible with two
553 distinct domes, and the olfactory bulbs widening on their anterior part. As the multivariate K
554 was lower than one, species resemble each other less than expected under a Brownian motion
555 model of evolution, which shows that, though significant, the phylogenetic signal remains
556 weak. This suggests that other factors, such as ecology, do affect the snake endocast
557 morphology.

558

559 **Ecological signal**

560 We also detected an ecological signal in the brain endocast of snakes, even when the
561 phylogenetic relationships were taken into account. Though the different ecologies tested here
562 are thus associated with morphological trends of the brain endocast, it nevertheless appears
563 difficult to associate one structure with one ecology. Both standard and phylogenetic
564 MANOVAs indicate significant differences between the ecologies, with an impact of all
565 variables on the distribution of snakes. Thus, fossorial species have a brain endocast with a

566 poor lateral development of the cerebral hemispheres, and not visible or absent optic tectum
567 and pituitary gland. Marine species exhibit an endocast more elongated, with cerebral
568 hemispheres poorly developed laterally and projected only in the antero-posterior plan, but the
569 optic tectum is clearly visible and the pituitary gland is developed ventrally. Brain endocasts
570 of terrestrial and arboreal snakes differ from marine ones' by the great lateral extension of the
571 cerebral hemispheres. Finally, it appears difficult to distinguish a common pattern for semi-
572 aquatic snakes.

573 Within the same ecology, a great variability in brain endocast morphology can be
574 observed. The results obtained from the outline curve analysis (Fig. 11 and 12) provide some
575 examples. The cerebral hemispheres of *Aipysurus duboisii* and *Aipysurus eydouxii* are wider
576 than long and developed ventrally on their posterior part, whereas in the other marine taxa of
577 our dataset, the cerebral hemispheres are as long as wide and only directed in the horizontal
578 plane. The brain endocasts of *Pelamis platurus* and *Candoia* sp. appear more flattened than
579 those respectively found in other marine and terrestrial species. Finally, the morphology, the
580 proportions and the orientation of the brain endocast of *Rhinotyphlops schlegelii* appear very
581 distinct from those found in other fossorial snakes. It appears difficult to interpret these
582 differences. It has been demonstrated that constraints imposed by the environment (e.g.,
583 habitat) and activity pattern have an impact in snake head shape, irrespective of the
584 phylogenetic relationships (Fabre et al., 2016; Segall et al., 2016). These ecological
585 constraints affect the brain endocast morphology in snakes as well. However, it is difficult to
586 determine with certainty which ecological parameters mostly affect the brain endocast
587 morphology. The two marine species, *A. duboisii* and *A. eydouxii*, have a brain endocast quite
588 different from other marine taxa. It is unclear if these differences are related to changes in
589 their skull morphology due to the fish-egg dietary specialization (Sanders et al., 2012) or if
590 the particular morphology of their cerebral hemispheres has a sensory meaning. Similarly, the

591 flattened brain endocast of *Pelamis platurus*, not found in any other marine specimen from
592 our dataset, could be related to modifications in the skull morphology associated with its
593 pelagic condition, only known in this species, or to its unique foraging strategy at the oceanic
594 surface through labile features such as slicks or drift lines (Brischoux & Lillywhite, 2011). It
595 will be interesting to decompose the ecology in different factors (e.g., locomotion, prey
596 capture mode) to determine which parameters mostly influence the snake brain endocast
597 morphology.

598

599 **Sensory inferences**

600 Studies in mammals and birds have shown that the endocast morphology, like the
601 brain morphology, may give some information about species sensory abilities (Sakai et al.,
602 2011a,b; Corfield et al., 2012, 2015; Carril et al., 2015). Several studies on snake brain have
603 shown a link between structure and function (e.g., Kubie et al., 1978; Halpern & Frumin,
604 1979; Halpern & Kubie, 1979; Friedman & Crews, 1985; Krohmer & Crews, 1987; Crews et
605 al., 1988; Miller & Gutzke, 1999; Wyneken, 2007; Krohmer et al., 2010) but the link between
606 sensory abilities and brain endocasts has never been investigated in snakes. According to
607 Starck (1979) and Nieuwenhuys et al. (1998), the brain of snakes could fill the majority of the
608 endocranial space, and thus reflect the brain anatomy. If it is the case, brain endocasts could
609 provide information about their sensory abilities. The relationships between the brain and the
610 brain endocast is currently untested in snakes (Olori, 2010), and was not the goal of this study.

611 In snakes, the main olfactory bulb (MOB) is responsible for capturing smells at the
612 level of the olfactory epithelium, and transmitting them to the olfactory bulb; the accessory
613 olfactory bulb (AOB) is responsible for pheromone processing related to chemical social
614 communication and prey capture (Bales, 2014). The MOB projects mainly to the lateral cortex
615 and the AOB mainly to the *nucleus sphericus* (Lanuza & Halpern, 1997), two structures

616 localized in the cerebral hemispheres. The MOB and AOB are involved in different
617 behavioral activities, such as predation, mating and courtship (Bales, 2014). It is difficult to
618 clearly identify the two structures and their limits from the brain endocast. However,
619 morphological differences are perceived between the sampled taxa and they may imply
620 differences in their sensory abilities. All snakes have a very developed vomeronasal system
621 (Kubie & Halpern, 1979; Bales, 2014); however in hydrophiinae sea snakes the main
622 olfactory bulbs are considered to be functionless and it seems that they use the AOB for
623 smelling underwater (Schwenk, 2008; Schichida et al., 2013). Brain endocasts of
624 hydrophiidae are indeed the only ones to show olfactory bulbs with a width increasing along
625 the antero-posterior axis (e.g., *Enhydrina schistosa*, see Fig. 5H), which could correspond to a
626 reduced MOB and a more developed AOB.

627 The cerebral hemispheres of snakes are composed of different structures (e.g., cortex,
628 nucleus sphericus, anterior ventricular ridge, amygdala), each being considered as a link
629 between the sources of sensory information and the brain structures that control and modulate
630 the behavior (Halpern, 1980; Bales, 2014). Different studies about the lizard brain have
631 shown that the medial dorsal cortices are relatively bigger in active foragers (Day et al.,
632 1999a,b; 2001; Ladage et al., 2009). In snakes, males, which have a larger average territory
633 than females, possess a significantly larger medial cortex than females (Roth et al., 2006).
634 However, all these internal structures are not distinguishable on endocasts. Moreover, no
635 comparative studies on snake brain endocasts have been performed to correlate size variation
636 of these inner neural structures with endocast morphology. It is thus difficult to evaluate
637 whether the different morphologies exhibited by the cerebral hemispheres of snakes involve
638 differences in their sensory abilities.

639 The optic tectum in snakes is involved in the production of natural orienting
640 movements in response to somatosensory, visual, and auditory stimuli (Nieuwenhuys et al.,

641 1998; Wyneken, 2007), and to signals from the infrared sensory system found in some snake
642 families (Boidae, Pythonidae, and Crotalinae) (Goris, 2011). Several authors have shown that
643 the size of the optic tectum is correlated to some behavioral traits and ecologies (Masai, 1973;
644 Nieuwenhuys et al., 1998). For instance diurnal species have a larger optic tectum than
645 burrowing species. From snake endocasts, it actually appears that all fossorial species have a
646 reduced optic tectum, (e.g., *Cylidrophis ruffus*, see Fig. 4C), contrary to terrestrial and
647 arboreal taxa, which have a large optic tectum (e.g., *Chrysopelea ornata*, see Fig. 4G).
648 According to Lillywhite (2014), vision is better developed in arboreal snakes, and poorly
649 developed in burrowing species and some aquatic species living in turbid waters. It seems
650 thus possible to connect the size of the optic tectum to the development of vision. According
651 to Masai (1973), the optic tectum of diurnal snakes is, as a rule, larger than that of nocturnal
652 ones. However, the correlation between large optic tectum and diurnal activity is not clear.
653 Some exceptions exist: the endocast of *Boiga dendrophila* (see Fig. 5B), a nocturnal snake
654 (Rodda et al., 1999; Shivik et al., 2000), also shows a large optic tectum. There seems also to
655 be no correlation between the occurrence of an infrared sensory system and the size of the
656 optic tectum on endocasts. Specimens that have infrared organs (e.g., *Crotalus atrox*, see Fig.
657 7B) do not exhibit a larger optic tectum than specimens without infrared organs (e.g., *Boa*
658 *constrictor*, see Fig. 7A). There is however one exception: *Erpeton tentaculatum* (see Fig. 6B-
659 D), the only specimen which has an endocast with the dorsal margin of the optic tectum
660 located more dorsally than the dorsal margin of the cerebral hemispheres. Such features can
661 be correlated to the special nature of *E. tentaculatum*, which is the only snake presenting a
662 pair of appendages that protrude from the face (Catania, 2011; 2012). The tentacles, useful to
663 detect and locate preys, are innervated by trigeminal fibers to the optic tectum and could be
664 responsible for its large size in *E. tentaculatum*.

665 Snake endocasts also show a great variability in the pituitary gland. This structure is
666 generally considered to be structurally and functionally the most complex organ of the
667 endocrine system (Harris & Donovan, 1966). Among vertebrates, the pituitary of snakes
668 possesses some unique features: an asymmetrical structure flattened dorsoventrally and a pars
669 tuberalis never developed (Schreibman, 1986). From the observation of brain endocasts only,
670 a large variability is observed. However, it is not possible to determine whether this
671 variability has a sensory significance. For example, brain endocasts of fossorial specimens
672 have a clearly reduced pituitary gland but it is not clear whether this morphology is an
673 adaptation reflecting the specialization of the skull due to fossorial activity (Rieppel, 1979;
674 Rieppel & Zaher, 2000) or if this morphology has a sensory implication.

675 It is tempting to interpret the brain endocast variability in snakes through differences
676 in sensory abilities between species; however, it is necessary to be very careful in the sensory
677 inferences brought by an endocast study, which gives only an overview of the external
678 morphology of the brain, and the complexity of the structure(s) must be taken into account.

679

680 **Perspectives**

681 The rapidly expanding interest in, and availability of, digital tomography data to
682 visualize casts of the vertebrate endocranial cavity housing the brain (endocasts) represent
683 new opportunities and challenges to the field of comparative neuroanatomy (Balanoff et al.,
684 2015). In snakes, the brain endocast is still poorly known and the information associated with
685 this structure remains untested. The different approaches used here have shown that snake
686 brain endocasts contain both phylogenetic and ecological signals. However, the degree of
687 influence of these two signals on the brain endocast morphology is difficult to interpret. It will
688 be interesting to dissociate the variability due to each signal. Moreover, to fully understand
689 the brain endocast structure and its variability among snakes, it appears necessary to

690 decompose the ecology in different parameters (e.g., locomotion, prey capture mode) in order
691 to test whether one is particularly associated to one brain endocast structure.

692 Beyond the methodological approaches that we used in this study, the resort to three-
693 dimensional geometric morphometrics (3DGM) would be interesting to improve the amount
694 of shape changes taken into consideration. However, the difficulty of finding homologous
695 anatomical landmarks would impose the use of sliding semi landmarks on surfaces (Gunz &
696 Mitteroecker, 2013).

697 Cranial endocasts also represent a potentially large amount of unexplored phylogenetic
698 data. Most morphological data for phylogenetic analyses of vertebrates come from the
699 exterior shape of the skull (e.g., Gauthier et al., 2012). Internal cranial morphology is poorly
700 represented in phylogenetic analyses because of the difficulty in visualizing and studying this
701 anatomy. The advent of CT technology provides the potential to incorporate these new data
702 into phylogenetic analyses.

703 Finally, in the context of the strong debate about the phylogenetic and ecological
704 origin of snakes (e.g., Lee et al., 1999; Conrad, 2008; Hsiang et al., 2015; Martill et al., 2015;
705 Reeder et al., 2015; Yi and Norell, 2015), endocranial studies might be of strong interest.
706 Their application on crown snakes and lineages closely related to snakes (i.e., varanids,
707 dibamids, mosasauroids) would provide major complementary information.

708

709 **Conclusion**

710 We used different methods to describe the brain endocast of snakes: descriptive
711 characters, outline curve analysis, measurement series, and we observed a great variability in
712 the brain endocast morphology of snakes. These methods provided different complementary
713 information but all have shown that the shape of this structure contains, as in mammals and
714 birds, a phylogenetic signal but also an ecological one. The different trends observed in the

715 brain endocast morphology distinguish the different ecologies, notably fossorial and marine
716 snakes. The great diversity observed in the brain endocast of snakes, even within the same
717 ecology, appears difficult to interpret and further analyses on the relation between brain
718 endocast and ecological and sensory factors will be required. Biological inferences based on
719 this structure should thus be made with caution and it is important to understand the
720 complexity of this structure in order to avoid quick potentially wrong assumptions.

721

722 **Acknowledgements**

723 This work was supported by a grant from Agence Nationale de la Recherche under the
724 LabEx ANR-10-LABX-0003-BCDiv, in the program “Investissements d’avenir” n° ANR-11-
725 IDEX-0004-02. We thank I. Ineich (MNHN, Paris, France), J. Rosado (MCZ, Harvard, U. S.
726 A), K. Lim (ZRC, National University of Singapore) and A. Herrel (MNHN, Paris, France)
727 for the loan of specimens and already digitized snake data. We thank the Steinmann-Institut
728 (Universität Bonn, Bonn, Germany), the UMS 2700 outils et méthodes de la systématique
729 intégrative CNRS-MNHN and AST-RX, Plateau technique d’accès scientifique à la
730 tomographie à rayons X du MNHN, and the ESRF (Grenoble, France; beamline ID17) and
731 Paul Tafforeau for providing beamtime and support. We are also thankful to the 3D platform
732 (UMR 7207, CR2P, MNHN) for giving access to the 3D imaging facilities. Finally, we want
733 to thank both reviewers for helpful comments and suggestions.

734

735 **Author contributions**

736 Research conception and design: A. H., N. B., P. V.

737 Data acquisition: A. H., R. A., R. B., G. D.

738 Data analysis and interpretation: A. H., R. A., R.C., Z. B.

739 Drafting of the manuscript: R. A.

740 Critical revision of the manuscript: All authors.

741

742 **Conflict of interest**

743 The authors declare no conflict of interest.

744

745 **References**

746 **Adams DC** (2014) A generalized K statistic for estimating phylogenetic signal from shape and
747 other high-dimensional multivariate data. *Systematic Biology* **63**, 685–697.

748 **Ahrens HE** (2014) Morphometric study of phylogenetic and ecologic signals in Procyonid
749 (Mammalia: Carnivora) endocasts: morphometrics of Procyonid endocasts. *The Anatomical*
750 *Record* **297**, 2318–2330.

751 **Anderson CL, Kabalka GW, Layne DG, Dyke JP, Burghardt GM** (2000) Noninvasive high
752 field MRI brain imaging of the Garter Snake (*Thamnophis sirtalis*). *Copeia*, **2000**, 265–269.

753 **Atobe Y, Nakano M, Kadota T et al.** (2004) Medullary efferent and afferent neurons of the facial
754 nerve of the Pit Viper *Gloydius brevicaudus*. *The journal of Comparative Neurology* **472**,
755 345–357.

756 **Aubret F, Bonnet X, Harris M, Maumelat S** (2005) Sex differences in body size and
757 ectoparasite load in the ball python, *Python regius*. *Journal of Herpetology* **39**, 315–320.

758 **Aurboonyawat T, Pereira V, Kring T et al.** (2008) Patterns of the Cranial Venous System from
759 the Comparative Anatomy in Vertebrates: Part II. The Lateral-Ventral Venous System.
760 *Interventional Neuroradiology*, **14**, 21–31.

761 **Balanoff AM, Bever GS, Colbert MW et al.** (2015) Best practices for digitally constructing
762 endocranial casts: examples from birds and their dinosaurian relatives. *Journal of Anatomy*
763 **229**, 173–190.

76 **Bales TB** (2014) Proliferation, migration and survival of cells in the telencephalon of the ball
765 python, *Python regius*. *PhD Thesis*, 131pp.

76 **Bever GS, Bell CJ, Maisano JA** (2005) The ossified braincase and cephalic osteoderms of
767 *Shinisaurus crocodilurus* (Squamata, Shinisauridae). *Palaeontologia Electronica* **8**, 1–36.

76 **Bienvenu T, Guy F, Coudyzer W et al.** (2011) Assessing endocranial variations in great apes and
769 humans using 3D data from virtual endocasts. *American Journal of Physical Anthropology*
770 **145**, 231–246.

77 **Blomberg SP, Garland T, Ives AR** (2003) Testing for phylogenetic signal in comparative data:
772 behavioral traits are more labile. *Evolution* **57**, 717–745.

77 **Boistel R, Swoger J, Krzic U et al.** (2011a) The future of three-dimensional microscopic imaging
774 in marine biology. *Marine Ecology* **32**, 438–452.

77 **Boistel R, Herrel A, Lebrun R et al.** (2011b) Shake rattle and roll: the bony labyrinth and aerial
776 descent in Squamates. *Integrative and Comparative Biology* **51**, 957–968.

77 **Bona P, Degrange FJ, Fernández MS** (2013) Skull anatomy of the bizarre Crocodylian
778 *Mourasuchus nativus* (Alligatoridae, Caimaninae): skull anatomy of *Mourasuchus nativus*.
779 *The Anatomical Record* **296**, 227–239.

78 **Brischoux F, Lillywhite HB** (2011) Light- and flotsam-dependent ‘float-and-wait’ foraging by
781 pelagic sea snakes (*Pelamis platurus*). *Marine Biology* **158**, 2343–2347.

78 **Butler AB, Hodos W** (2005) Comparative Vertebrate Neuroanatomy: Evolution and Adaptation.
783 *John Wiley & Sons, Inc., Hoboken, NJ, USA*, 744 pp.

78 **Carril J, Tambussi CP, Degrange FJ, Benitez Saldivar MJ, Picasso MBJ** (2015) Comparative
785 brain morphology of Neotropical parrots (Aves, Psittaciformes) inferred from virtual 3D
786 endocasts. *Journal of Anatomy* **229**, 1–13.

78 **Catania KC** (2011) The brain and behavior of the tentacled snake. *Annals of the New York*
788 *Academy of Sciences* **1225**, 83–89.

78 **Catania KC** (2012) Tactile sensing in specialized predators – from behavior to the brain. *Current*
790 *Opinion in Neurobiology* **22**, 251–258.

79 **Chapla ME, Nowacek DP, Rommel SA, Sadler VM** (2007) CT scans and 3D reconstructions of
792 Florida manatee (*Trichechus manatus latirostris*) heads and ear bones. *Hearing Research* **228**,
793 123–135.

79 **Christensen CB, Christensen-Dalsgaard J, Brandt C, Teglberg Madsen P** (2012) Hearing with
795 an atympanic ear: good vibration and poor sound-pressure detection in the royal python,
796 *Python regius*. *The Journal of Experimental Biology* **215**, 331–342.

79 **Comeaux RS, Olori JC, Bell CJ** (2010) Cranial osteology and preliminary phylogenetic
798 assessment of *Plectrurus aureus* Beddome, 1880 (Squamata: Serpentes: Uropeltidae).
799 *Zoological Journal of the Linnean Society* **160**, 118–138.

80 **Conrad JL** (2008) Phylogeny and systematics of Squamata (Reptilia) based on morphology.
801 *Bulletin of the American Museum of Natural History* **310**, 1–182.

80 **Corfield JR, Wild JM, Parsons S, Kubke MF** (2012) Morphometric analysis of telencephalic
803 structure in a variety of Neognath and Paleognath bird species reveals regional differences
804 associated with specific behavioral traits. *Brain, Behavior and Evolution* **80**, 181–195.

80 **Corfield JR, Price K, Iwaniuk A et al.** (2015) Diversity in olfactory bulb size in birds reflects
806 allometry, ecology and phylogeny. *Frontiers in Neuroanatomy* **9**,
807 doi:10.3389/fnana.2015.00102.

80 **Crews D, Hingorani V, Nelson RJ** (1988) Role of the pineal gland in the control of annual
809 reproductive behavioral and physiological cycles in the Red-Sided Garter Snake (*Thamnophis*
810 *sirtalis parietalis*). *Journal of Biological Rhythms* **3**, 293–302.

81 **Danilo L, Remy J, Vianey-Liaud M, Mérigeaud S, Lihoreau F** (2015) Intraspecific variation of
812 endocranial structures in extant Equus: A prelude to endocranial studies in fossil Equoids.
813 *Journal of Mammalian Evolution* **22**, 561–582.

81 **Day LB, Crews D, Wilczynski W** (1999a) Relative medial and dorsal cortex volume in relation to
815 foraging strategy in congeneric lizards. *Brain, Behavior and Evolution* **54**, 314–322.

81 **Day LB, Crews D, Wilczynski W** (1999b) Spatial and reversal learning in congeneric lizards with
817 different foraging strategies. *Animal Behaviour* **57**, 395–407.

81 **Day LB, Crews D, Wilczynski W** (2001) Effects of medial and dorsal cortex lesions on spatial
819 memory in lizards. *Behavioural Brain Research* **118**, 27–42.

82 **Ekdale EG** (2010) Ontogenetic variation in the bony labyrinth of *Monodelphis domestica*
821 (Mammalia: Marsupialia) following ossification of the inner ear cavities. *The Anatomical*
822 *Record: Advances in Integrative Anatomy and Evolutionary Biology* **293**, 1896–1912.

82 **Ekdale EG** (2011) Morphological variation in the ear region of pleistocene elephantimorpha
824 (Mammalia, Proboscidea) from central Texas. *Journal of Morphology* **272**, 452–464.

82 **Ekdale EG** (2013) Comparative anatomy of the bony labyrinth (inner ear) of placental mammals.
826 *PLoS One* **8**, e66624.

82 **Fabre A-C, Bickford D, Segall M, Herrel A** (2016) The impact of diet, habitat use, and
828 behaviour on head shape evolution in homalopsid snakes. *Biological Journal of the Linnean*
829 *Society* **118**, 634–647.

83 **Friedman D, Crews D** (1985) Role of the anterior hypothalamus–preoptic area in the regulation of
831 courtship behavior in the male Canadian red-sided garter snake (*Thamnophis sirtalis*
832 *parietalis*): Lesion experiments. *Behavioral neuroscience* **99**, 942–949.

83 **Gauthier JA, Kearney M, Maisano JA, Rieppel O, Behlke ADB** (2012) Assembling the
834 squamate tree of life: Perspectives from the phenotype and the fossil record. *Bulletin of the*
835 *Peabody Museum of Natural History* **53**, 3–308.

83 **George ID, Holliday CM** (2013) Trigeminal nerve morphology in *Alligator mississippiensis* and
837 its significance for Crocodyliform facial sensation and evolution. *The Anatomical Record* **296**,
838 670–680.

836 **Georgi JA, Sipla J** (2008) Comparative and functional anatomy of balance in aquatic reptiles and
840 birds. In *Sensory Evolution on the Threshold: Adaptations in Secondarily Aquatic*
841 *Vertebrates*, Thewissen JMG, Numella S. Berkeley: University of California Press. pp. 233–
842 256.

846 **Gonzales LA, Benefit BR, McCrossin ML, Spoor F** (2015) Cerebral complexity preceded
844 enlarged brain size and reduced olfactory bulbs in Old World monkeys. *Nature*
845 *Communications* **6**, 1-9.

846 **Goris RC** (2011) Infrared organs of snakes: An integral part of vision. *Journal of Herpetology* **45**,
847 2–14.

846 **Greene HW, Fogden M, Fogden P** (2000) Snakes: The Evolution of Mystery in Nature.
849 *University of California Press*, 365pp.

85 **Gunz P, Mitteroecker P** (2013) Semilandmarks: a method for quantifying curves and surfaces.
851 *Hystrix, the Italian Journal of Mammalogy* **24**, 103–109.

85 **Halpern M** (1980) The telencephalon of snakes. In S. O. E. Ebbesson (ed) *Comparative*
853 *Neurology of the telencephalon*. Springer US, 257–295.

85 **Halpern M, Frumin N** (1979) Roles of the vomeronasal and olfactory system in prey attack and
855 feeding garter snakes. *Physiology & Behavior* **22**, 1183–1189.

85 **Halpern M, Kubie JL** (1980) Chemical access to the vomeronasal organs of Garter snakes.
857 *Physiology & Behavior* **24**, 367–371.

85 **Harris GW, Donovan BT** (1966) The pituitary gland: anterior pituitary. *University of California*
859 *Press*, 444–459.

86 **Heatwole H** (1999) Sea snakes. *Krieger Publishing Company*, 148pp.

86 **Hoogland PV** (1982) Brainstem afferents to the thalamus in a lizard, *Varanus exanthematicus*. *The*
862 *journal of Comparative Neurology* **210**, 152–162.

- 86**Hopson JA** (1979) Paleoneurology. In C. Gans, R.G. Northcutt and P. Ulinski (eds) *Biology of the*
864 *Reptilia (Neurology A)*. Academic Press, New York 9, 39–146.
- 86**Houssaye A, Boistel R, Böhme W, Herrel A** (2013) Jack-of-all-trades master of all? Snake
866 vertebrae have a generalist inner organization. *Naturwissenschaften* **100**, 997–1006.
- 86**Hsiang AY, Field DJ, Webster TH et al.** (2015) The origin of snakes: revealing the ecology,
868 behavior, and evolutionary history of early snakes using genomics, phenomics, and the fossil
869 record. *BMC Evolutionary Biology* **15**, 1–22.
- 87**Hurlburt GR, Ridgely RC, Witmer LM** (2013) Relative size of brain and cerebrum in
871 tyrannosaurid dinosaurs: an analysis using brain-endocast quantitative relationships in extant
872 alligators. In Parrish JM, Molnar RE, Currie PJ, Koppelhus EB (eds) *Tyrannosaurid*
873 *Paleobiology*, Bloomington: Indiana University Press, 1–21.
- 87**Jerison H** (1973) Evolution of the brain and intelligence. Academic Press, New York, 482 pp.
- 87**Kawabe S, Shimokawa T, Miki H, Matsuda S, Endo H** (2013) Variation in avian brain shape:
876 relationship with size and orbital shape. *Journal of Anatomy* **223**, 495–508.
- 87**Kawabe S, Matsuda S, Tsunekawa N, Endo H** (2015) Ontogenetic shape change in the chicken
878 brain: Implications for paleontology. *PLOS ONE* **10**, e0129939.
- 87**Kim R, Evans D** (2014) Relationships among brain, endocranial cavity, and body sizes in reptiles.
880 *Society of Vertebrate Paleontology 74th Annual Meeting*, Berlin, Germany.
- 88**Krohmer RW, Crews D** (1987) Temperature activation of courtship behavior in the male red-
882 sided garter snake (*Thamnophis sirtalis parietalis*): Role of the anterior hypothalamus-
883 preoptic area. *Behavioral neuroscience* **101**, 228–236.
- 88**Krohmer RW, Boyle MH, Lutterschmidt DI, Mason RT** (2010) Seasonal aromatase activity in
885 the brain of the male red-sided garter snake. *Hormones and Behavior* **58**, 485–492.

- 886 **Kubie JL, Vagvolgyi A, Halpern M** (1978) Roles of the vomeronasal and olfactory systems in
887 courtship behavior of male garter snakes. *Journal of Comparative and Physiological*
888 *Psychology* **92**, 627–641.
- 889 **Kubie JL, Halpern M** (1979) Chemical senses involved in Garter snake prey trailing. *Journal of*
890 *Comparative and Physiological Psychology* **93**, 648–667.
- 891 **Ladage LD, Riggs BJ, Sinervo B, Pravosudov VV** (2009) Dorsal cortex volume in male side-
892 blotched lizards (*Uta stansburiana*) is associated with different space use strategies. *Animal*
893 *behaviour* **78**, 91–96.
- 894 **Lanuza E, Halpern M** (1997) Afferent and efferent connections of the nucleus sphericus in the
895 snake *Thamnophis sirtalis*: Convergence of olfactory and vomeronasal information in the
896 lateral cortex and the amygdala. *The journal of Comparative Neurology* **385**, 627–640.
- 897 **Lee MS, Scanlon JD** (2002) Snake phylogeny based on osteology, soft anatomy and ecology.
898 *Biological Review* **77**, 333–401.
- 899 **Lee MS, Bell Jr. GL, Caldwell MW** (1999) The origin of snake feeding. *Nature* **400**, 655–659.
- 900 **Lefebvre L, Reader SM, Sol D** (2004) Brains, innovations and evolution in birds and primates.
901 *Brain, Behavior and Evolution* **63**, 233–246.
- 902 **Lillywhite HB** (2014) How snakes work: structure, function, and behavior of the world's snakes.
903 *Oxford University Press*, 256pp.
- 904 **Lyras GA, Van Der Geer AAE** (2003) External brain anatomy in relation to the phylogeny of
905 Caninae (Carnivora: Canidae). *Zoological Journal of the Linnean Society* **138**, 505–522.
- 906 **Macrini TE, Rowe T, VandeBerg JL** (2007) Cranial endocasts from a growth series of
907 *Monodelphis domestica* (Didelphidae, Marsupialia): A study of individual and ontogenetic
908 variation. *Journal of Morphology* **268**, 844–865.
- 909 **Martill DM, Tischlinger H, Longrich NR** (2015) A four-legged snake from the Early Cretaceous
910 of Gondwana. *Science* **349**, 416–419.

91 **Martinez-Garcia F, Olucha FE, Teruel V, Lorente MJ, Schwerdtfeger WK** (1991) Afferent
912 and efferent connections of the olfactory bulbs in the lizard *Podarcis hispanica*. *The journal*
913 *of Comparative Neurology* **305**, 337–347.

91 **Masai H** (1973) Structural patterns of the optic tectum in Japanese snakes of the family Colubridae
915 in relation to habit. *Journal Für Hirnforschung* **14**, 367–374.

91 **Miller LR, Gutzke WHN** (1999) The role of the vomeronasal organ of crotalines (Reptilia:
917 Serpentes: Viperidae) in predator detection. *Animal Behaviour* **58**, 53–57.

91 **Mosimann JE, James FC** (1979) New Statistical Methods for Allometry with Application to
919 Florida Red-Winged Blackbirds. *Evolution* **33**, 444–459.

92 **Nieuwenhuys R, ten Donkelaar HJ, Nicholson C** (1998) *The Central Nervous System of*
921 *Vertebrates*. Berlin: Springer, 2214pp.

92 **Northcutt RG** (2002) Understanding Vertebrate Brain Evolution. *Integrative and Comparative*
923 *Biology* **42**, 743–756.

92 **Olori JC** (2010) Digital Endocasts of the Cranial Cavity and Osseous Labyrinth of the Burrowing
925 Snake *Uropeltis woodmasoni* (Alethinophidia: Uropeltidae). *Copeia* **2010**, 14–26.

92 **Porter WR, Witmer LM** (2015) Vascular Patterns in Iguanas and Other Squamates: Blood
927 Vessels and Sites of Thermal Exchange. *PLOS ONE* **10**, e0139215.

92 **Powell BJ, Leal M** (2014) Brain Organization and Habitat Complexity in Anolis Lizards. *Brain*
929 *Behavior and Evolution* **84**, 8–18.

93 **Dyron RA, Burbrink FT, Colli GR et al.** (2011) The phylogeny of advanced snakes
931 (Colubroidea), with discovery of a new subfamily and comparison of support methods for
932 likelihood trees. *Molecular Phylogenetics and Evolution* **58**, 329–342.

93 **R Development Core Team** (2008) R: A language and environment for statistical computing. R
934 Foundation for Statistical Computing, Vienna, Austria. ISBN 3-900051-07-0, [http://www.R-](http://www.R-project.org)
935 [project.org](http://www.R-project.org).

93 **Racicot RA, Colbert MW** (2013) Morphology and Variation in Porpoise (Cetacea: Phocoenidae)
937 Cranial Endocasts. *The Anatomical Record* **296**, 979–992.

93 **Reeder TW, Townsend TM, Mulcahy DG et al.** (2015) Integrated analyses resolve conflicts over
939 squamate reptile phylogeny and reveal unexpected placements for fossil taxa. *PLOS ONE* **10**,
940 e0118199.

94 **Reperant J, Rio J-P, Ward R et al.** (1992) Comparative Analysis of the Primary Visual System
942 of Reptiles. In C. Gans and P. S. Ulinski (eds) *Sensory Integration. Biology of Reptilia,*
943 *(Neurology C)*. The University of Chicago Press **7**, 175–240.

94 **Rieppel O** (1979) The braincase of Typhlops and Leptotyphlops (Reptilia: Serpentes). *Zoological*
945 *Journal of the Linnean Society* **65**, 161–176.

94 **Rieppel O, Zaher H** (2000) The braincases of mosasaurs and Varanus, and the relationships of
947 snakes. *Zoological Journal of the Linnean Society* **129**, 489–514.

94 **Rieppel O, Maisano JA** (2007) The skull of the rare Malaysian snake *Anomochilus leonardi*
949 Smith, based on high-resolution X-ray computed tomography. *Zoological Journal of the*
950 *Linnean Society* **149**, 671–685.

95 **Rodda GH, Fritts TH, McCoid MJ, Campbell III EW** (1999) An Overview of the Biology of
952 the Brown Treesnake (*Boiga irregularis*), a Costly Introduced Pest on Pacific Islands. In
953 Rodda, G. H., Sawai, Y.; Chiszar, D. & Tanaka, H. (eds) *Problem snake management: the*
954 *habu and the brown treesnake*. Cornell University Press, Ithaca, NY, 534pp.

95 **Rohlf FJ, Slice D** (1990) Extensions of the Procrustes method for the optimal superimposition of
956 landmarks. *Systematic Biology* **39**, 40–59.

95 **Roth ED, Lutterschmidt WI, Wilson DA** (2006) Relative Medial and Dorsal Cortex Volume in
958 Relation to Sex Differences in Spatial Ecology of a Snake Population. *Brain Behavior and*
959 *Evolution* **67**, 103–110.

- 96 **Rowe T, Brochu CA, Colbert M et al.** (1999) Introduction to Alligator: Digital atlas of the skull.
961 *Journal of Vertebrate Paleontology* **19**, 1–8.
- 96 **Sakai ST, Arsznov BM, Lundrigan BL, Holekamp KE** (2011a) Brain Size and Social
963 Complexity: A Computed Tomography Study in Hyaenidae. *Brain, Behavior and Evolution*
964 **77**, 91–104.
- 96 **Sakai ST, Arsznov BM, Lundrigan BL, Holekamp KE** (2011b) Virtual endocasts: an
966 application of computed tomography in the study of brain variation among hyenas: Hyena
967 endocasts. *Annals of the New York Academy of Sciences* **1225**, 160–170.
- 96 **Sanders KL, Rasmussen AR, Elmberg J et al.** (2012) *Aipysurus mosaicus*, a new species of egg-
969 eating sea snake (Elapidae: Hydrophiinae), with a redescription of *Aipysurus eydouxii* (Gray,
970 1849). *Zootaxa* **3431**, 1–18.
- 97 **Schreibman MP** (1986) The Pituitary Gland. In: Pang PKT, Schreibman MP (eds) *Vertebrate*
972 *Endocrinology: Fundamentals and Biomedical Implications*, Vol. I. Academic Press, New
973 York, 11–55.
- 97 **Schwenk K** (2008) Comparative anatomy and physiology of chemical senses in nonavian aquatic
975 reptiles. In Thewissen, J.G.M., Nummela, S. (eds.) *Sensory Evolution on the Threshold:*
976 *Adaptations in Secondarily Aquatic Vertebrates*. *University of California Press, California*,
977 65–81.
- 97 **Segall M, Cornette R, Fabre A-C, Godoy-Diana R, Herrel A** (2016) Does aquatic foraging
979 impact head shape evolution in snakes? *Proceedings of the Royal Society B* **283**, 1–7.
- 98 **Senn DG** (1966) Über das optische System im Gehirn squamater Reptilien. Eine vergleichend-
981 morphologische Untersuchung, unter besonderer Berücksichtigung einiger Wühlschlangen.
982 *Acta Anatomica. Supplementum* **52**, 1–87.
- 98 **Senn DG, Northcutt RG** (1973) The Forebrain and Midbrain of Some Squamates and Their
984 Bearing on the Origin of Snakes. *Journal of Morphology* **140**, 135–152.

- 988 **Shichida Y, Yamashita T, Imai H, Kishida T** (2013) Evolution and Senses: Opsins, Bitter Taste,
986 and Olfaction. Berlin, Germany: Springer, 46pp.
- 988 **Shivik JA, Wright WG, Clark L** (2000) Seasonal variability in brown tree snake (*Boiga*
988 *irregularis*) response to lures. *Canadian Journal of Zoology* **78**, 79–84.
- 988 **Smeets WJA, Hoogland PV, Lohman AH** (1986) A Forebrain Atlas of the Lizard Gekko gekko.
990 *The journal of Comparative Neurology* **254**, 1–19.
- 992 **Smith NA, Clarke JA** (2012) Endocranial Anatomy of the Charadriiformes: Sensory System
992 Variation and the Evolution of Wing-Propelled Diving. *PLoS ONE* **7**, e49584.
- 992 **Souza NM, Maggs DJ, Park SA et al.** (2015) Gross, histologic, and micro-computed tomographic
994 anatomy of the lacrimal system of snakes. *Veterinary Ophthalmology* **18**, 15–22.
- 992 **Starck D** (1979) Cranio-Cerebral Relations in Recent Reptiles. In Gans, C., Northcutt, R.G.,
996 Ulinski, P. (eds) *Biology of the Reptilia (Neurology A)*, Academic Press, London, New York
997 and San Francisco, 462 pp.
- 992 **Walsh SA, Barrett PM, Milner AC, Manley G, Witmer LM** (2009) Inner ear anatomy is a
999 proxy for deducing auditory capability and behaviour in reptiles and birds. *Proceedings of the*
1000 *Royal Society B: Biological Sciences* **276**, 1355–1360.
- 1002 **Walsh SA, Knoll MA** (2011) Directions in Palaeoneurology. *The Palaeontological Association*
1002 **86**, 263–279.
- 1002 **Walsh SA, Milner A** (2011) Evolution of the Avian Brain and Senses. In G. Dyke and G. Kaiser
1004 (eds) *Living Dinosaurs: The Evolutionary History of Modern Birds*, First Edition. Published
1005 by John Wiley & Sons, 282–305.
- 1002 **Willis KL, Christensen-Dalsgaard J, Ketten DR, Carr CE** (2013) Middle Ear Cavity
1007 Morphology Is Consistent with an Aquatic Origin for Testudines. *PLoS ONE* **8**, e54086.
- 1002 **Witmer LM, Ridgely RC, Dufeu DL, Semones MC** (2008) Using CT to Peer into the Past: 3D
1009 Visualization of the Brain and Ear Regions of Birds, Crocodiles, and Nonavian Dinosaurs. In:

1010 Frey R, Endo H, editors. Anatomical Imaging: Towards a New Morphology. Tokyo. Springer-
1011 Verlag, 67–87.

1012 **Wynneken J** (2007) Reptilian Neurology: Anatomy and Function. *Veterinary Clinics of North*
1013 *America: Exotic Animal Practice* **10**, 837–853.

1014 **Yi H, Norell MA** (2015) The burrowing origin of modern snakes. *Science Advances* **1**, e1500743.

1015 **Zelditch ML, Swiderski DL, Sheets HD, Fink WL** (2004) Geometric morphometrics for
1016 biologists: a primer. Academic Press, 443pp.

1017

1018 **Supporting information**

1019 Appendix S1. Table of measurements taken on snake endocasts

1020 Appendix S2. Table of measurements taken on the three *Python regius* specimens

1021 Appendix S3. List of characters and matrix used for the PCoA

1022 Appendix S4. Distribution of the variables in the principal component analyses performed on
1023 the 45 snake specimens.

1024

1025

1026

1027

1028

1029

1030

1031

1032

1033

1034

1035 **Tables**

1036 **Table 1.** List of the material analyzed. Ha represents the categories based on habitat: A,
 1037 arboreal; F, fossorial; M, marine; T, terrestrial; SA, semi-aquatic. AH, Anthony Herrel
 1038 personal collections; GD, Gheylan Daghfous personal collections.

1039

Family	Taxon	Ab.	Ha	Collection reference	Voxel size
Boidae	<i>Rhinotyphlops schlegelii</i>	Rs	F	AH Unnumb	13.3
Anomalepididae	<i>Typhlophis squamosus</i>	Ts	F	MNHN 1997.2042	5.1
Uropeltidae	<i>Uropeltis pulneyensis</i>	Up	F	MNHN 1994.0753	5.0
Cylindrophiiidae	<i>Cylindrophis ruffus</i>	Cy	F	MNHN 1998.0201	20.1
Aniliidae	<i>Anilius scytale</i>	An	F	MNHN 1997.2106	10.1
Pythonidae	<i>Python regius</i>	P3	T	AH Unnumb	33.3
	<i>Python regius</i>	P2	T	AH Unnumb	28.9
	<i>Python regius</i>	P1	T	AH MS 37	21.6
Boidae	<i>Boa constrictor</i>	Bc	A	MNHN 1989.0177	7.6
	<i>Candoia</i> sp.	Cd	T	AH Unnumb	33.3
	<i>Corallus hortulanus</i>	Ch	A	AH MS 62	32
	<i>Eunectes murinus</i>	Em	SA	MNHN 1996.7898	7.6
Acrochordidae	<i>Acrochordus granulatus</i>	Ag	SA	ZRC 2.2334	24.2
Pareatidae	<i>Pareas margaritophorus</i>	Pm	A	MNHN 1974.1469	7.5
Viperidae	<i>Crotalus atrox</i>	Cr	T	AH MS 31	28.5
	<i>Agkistrodon contortrix</i>	Ac	T	AH MS 56	23.4
Homalopsidae	<i>Enhydris enhydris</i>	Ee	SA	ZRC 2.5507b	24.2
	<i>Enhydris punctata</i>	Ep	SA	ZRC 2.3554	24.2
	<i>Cerberus rynchops</i>	Ce	SA	MNHN-RA-1998.8583	35.3
	<i>Homalopsis buccata</i>	Hb	SA	ZRC 2.6411	24.2
	<i>Erpeton tentaculatum</i>	Et	SA	GD pers. coll.	7.5
	<i>Bitia hydroides</i>	Bh	M	ZRC 2.4374	20.9
	<i>Fordonia leucobalia</i>	Fl	SA	MNHN-RA-1912.26	33.2
	<i>Cantoria violacea</i>	Cv	SA	ZRC 2.3672	20.8
Lamprophiidae	<i>Mimophis mahfalensis</i>	Mm	T	MRSN R3171	24.7
	<i>Atractaspis irregularis</i>	Ai	F	MNHN 1999.9129	7.6
Elapidae	<i>Micrurus lemniscatus</i>	Ml	T	MNHN 1997.2353	7.6
	<i>Naja nivea</i>	Nn	T	AH MS 68	28.5
	<i>Hydrophis elegans</i>	He	M	MNHN-RA-0.1879	30.7
	<i>Enhydrina schistosa</i>	Es	M	ZRC 2.2043	20.8
	<i>Astrotia stokesii</i>	As	M	ZRC 2.2032	20.8

	<i>Hydrophis major</i>	Hm	M	MNHN 1990 4557	44.8
	<i>Hydrophis ornatus</i>	Ho	M	MNHN-RA-1994.6997	36
	<i>Pelamis platurus</i>	Pp	M	AH MS 64	31.9
	<i>Aipysurus duboisii</i>	Ad	M	MNHN-RA-1990.4519	41
	<i>Aipysurus eydouxi</i>	Ae	M	MNHN-RA-0.7704	40.2
	<i>Microcephalophis gracilis</i>	Mg	M	ZRC 2.2155	20.8
Natricidae	<i>Thamnophis sirtalis</i>	Ta	T	GD pers. coll.	7.5
Colubridae	<i>Chrysopelea ornata</i>	Co	A	MCZ R-177291	14.9
	<i>Hierophis gemonensis</i>	Hg	T	AH Unnumb	23.4
	<i>Hierophis viridiflavus</i>	Hv	T	AH Unnumb	19.2
	<i>Dispholidus typus</i>	Dt	A	AH Unnumb	32
	<i>Boiga dendrophila</i>	Bd	A	AH MS 102	18.2
	<i>Dasypeltis</i> sp.	Ds	A	MCZ 71877	14.9
	<i>Coronella austriaca</i>	Ca	T	AH MS 51	21.6

1040

1041

1042

1043

1044

1045

1046

1047

1048

1049

1050

1051

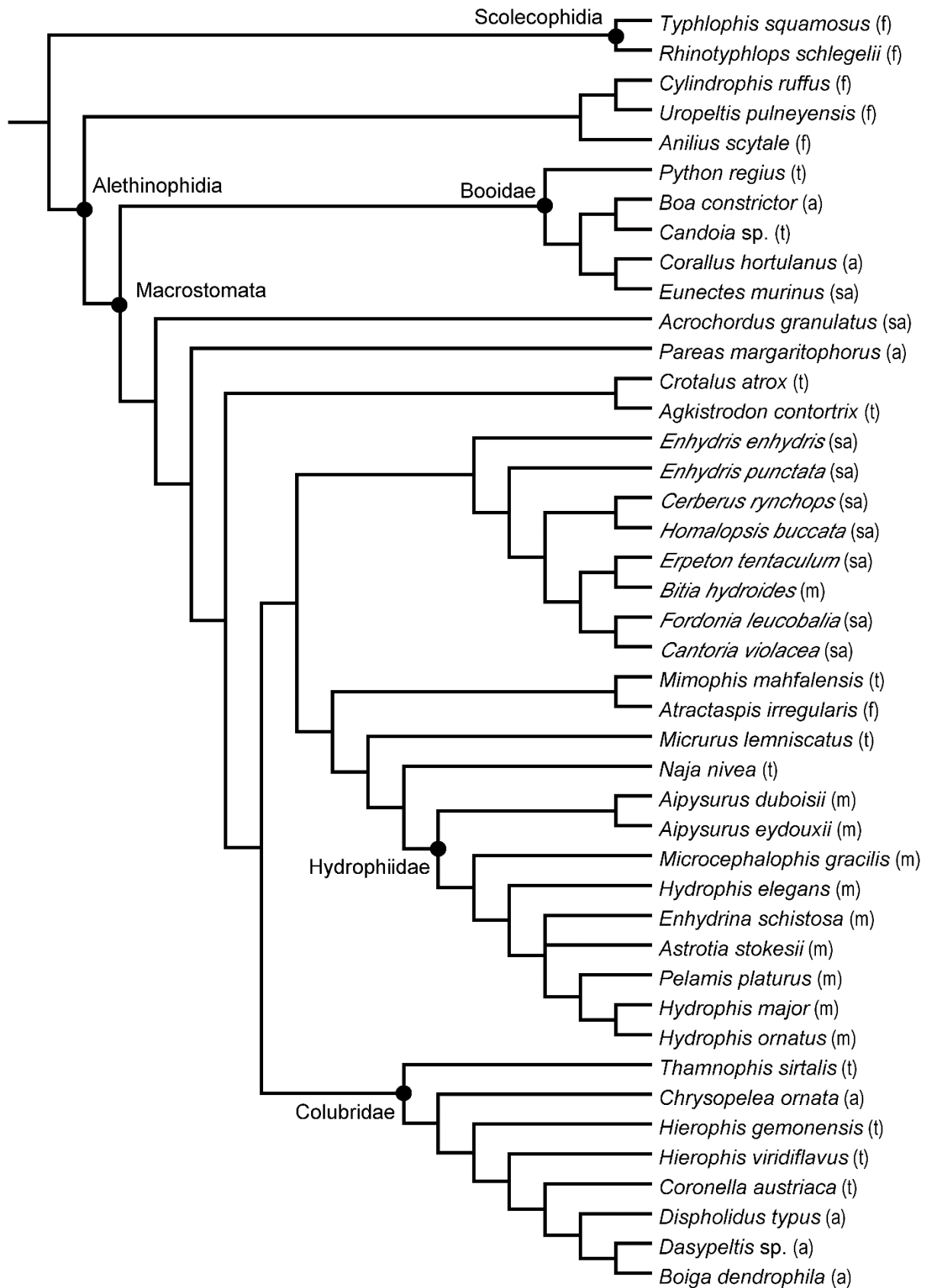
1052

1053

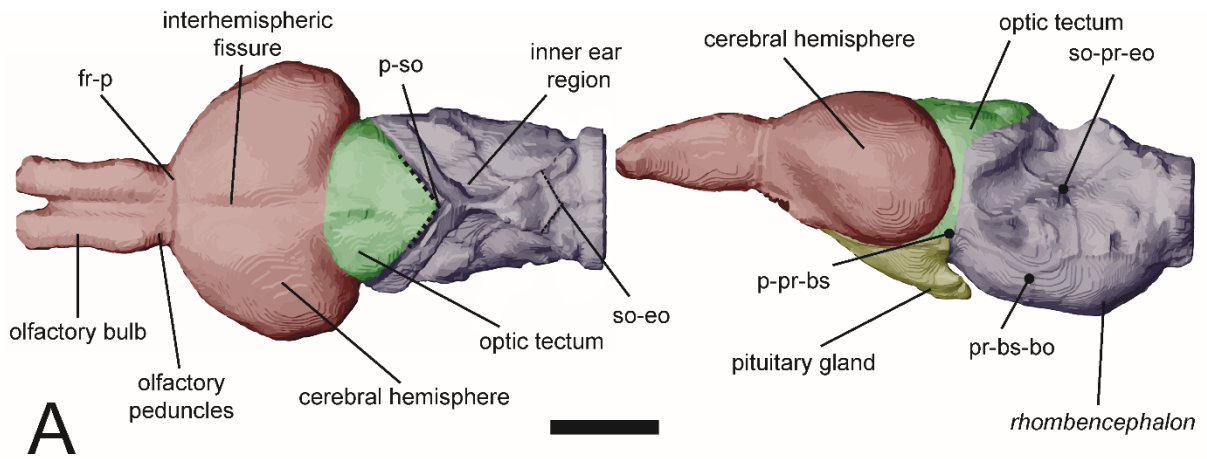
1054

1055

1056

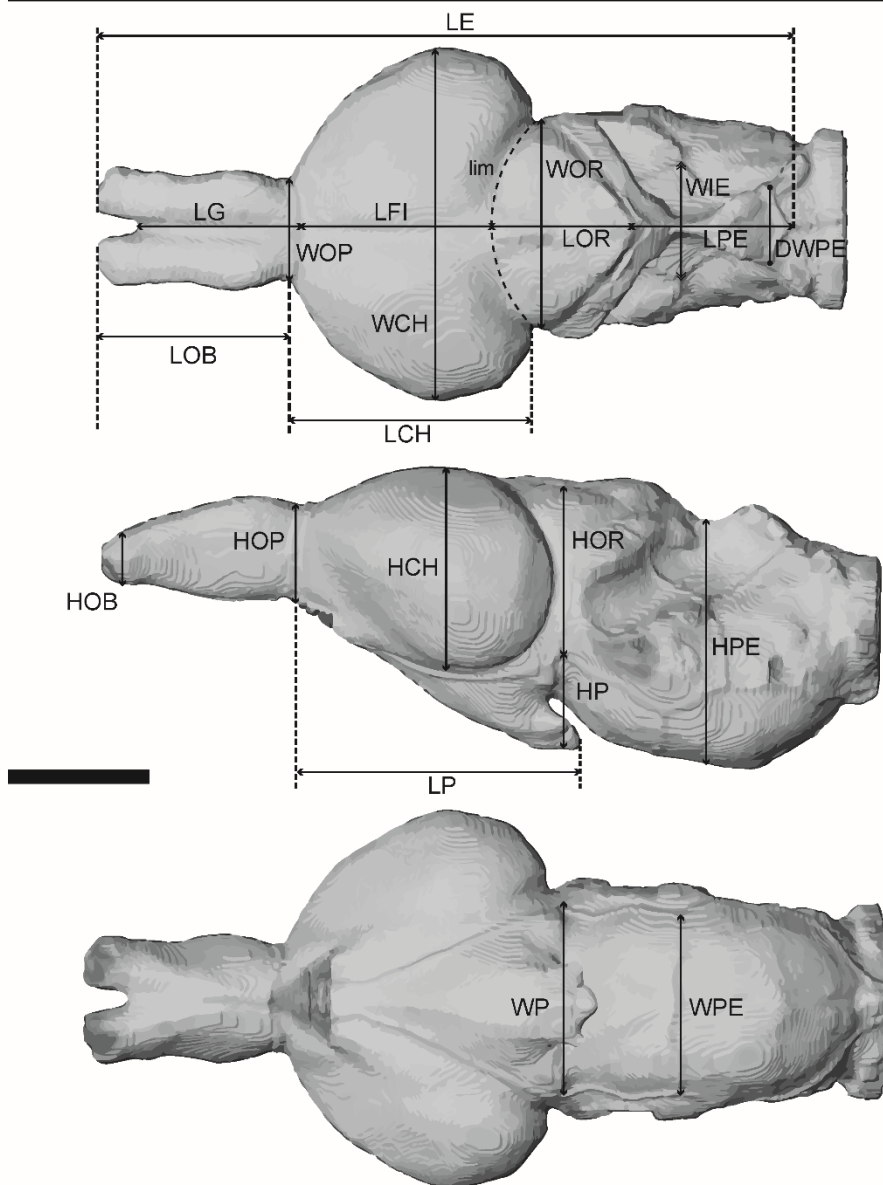


1058 **Fig. 1.** Schematic phylogenetic relationships of snakes sampled in the study (modified from
1059 Pyron et al., 2011; Hsiang et al., 2015; Lee and Scanlon, 2002). Principal ecology/habitat:
1060 fossorial (f), terrestrial (t), arboreal (a), semi-aquatic (sa), marine (m).
1061



A

B

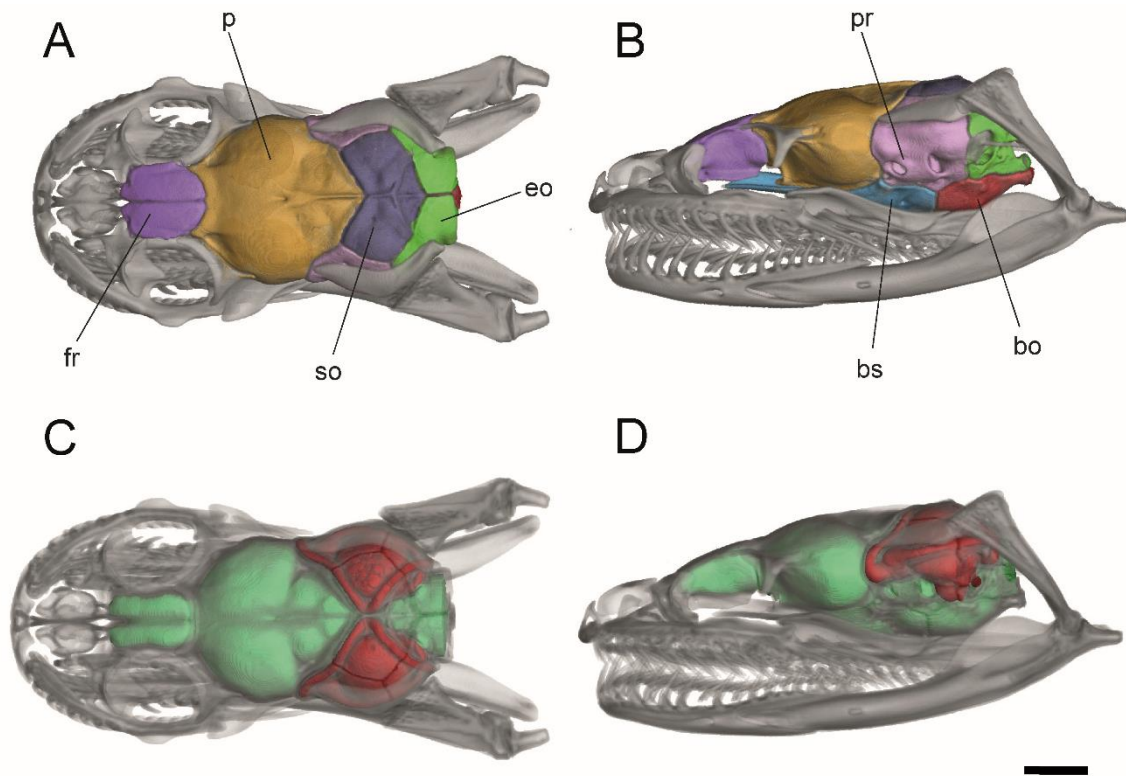


1062

1063

1064 **Fig. 2.** Reconstructed brain endocast of *Enhydria punctata* (Homalopsidae) (**A**), Illustration of
1065 the major structures seen in dorsal and left lateral views: telencephalon (red), diencephalon
1066 (yellow), mesencephalon (green), rhombencephalon (purple); (**B**), Illustration of the various
1067 measurements defined in Material and Method and taken in dorsal, left lateral and ventral
1068 views. **Abbreviations:** **fr-p**, fronto-parietal suture; **lim**, groove between the optic tectum and
1069 the cerebral hemispheres; **p-pr-bs**, triple point formed by the sutures between the parietal,
1070 prootic and basisphenoid; **p-so**, parietal-supraoccipital suture; **pr-bs-bo**, triple point formed
1071 by the suture between the prootic, basisphenoid and basioccipital; **so-eo**, supraoccipital-
1072 exoccipital suture; **so-pr-eo**, triple point formed by the sutures of the supraoccipital, prootic
1073 and exoccipital; **DWPE**, Dorsal width of the posterior end of the brain endocast; **HCH**,
1074 Maximal height of the cerebral hemisphere; **HOB**, Height of the main olfactory bulb; **HOP**,
1075 Height of the olfactory peduncle; **HOR**, Height of the optic tectum; **HP**, Height of the
1076 pituitary bulb; **HPE**, Height of the posterior part of the brain endocast; **LCH**, Lateral
1077 expansion of the cerebral hemispheres; **LE**, Length of the brain endocast; **LFI**, Length of the
1078 interhemispheric fissure; **LG**, Length of the groove between olfactory bulbs; **LOB**, Length of
1079 the olfactory bulbs; **LOR**, Length of the optic tectum; **LP**, Length of the pituitary bulb; **LPE**,
1080 Length of the posterior part of the brain endocast; **WCH**, Maximal width of the cerebral
1081 hemispheres; **WIE**, Width in the inner ear region; **WOP**, Width of the olfactory peduncles;
1082 **WOR**, Maximal width of the optic tectum; **WP**, Width in the pituitary gland region; **WPE**,
1083 Width of the ventral part of the brain endocast. Scale bar equals to 2 mm.

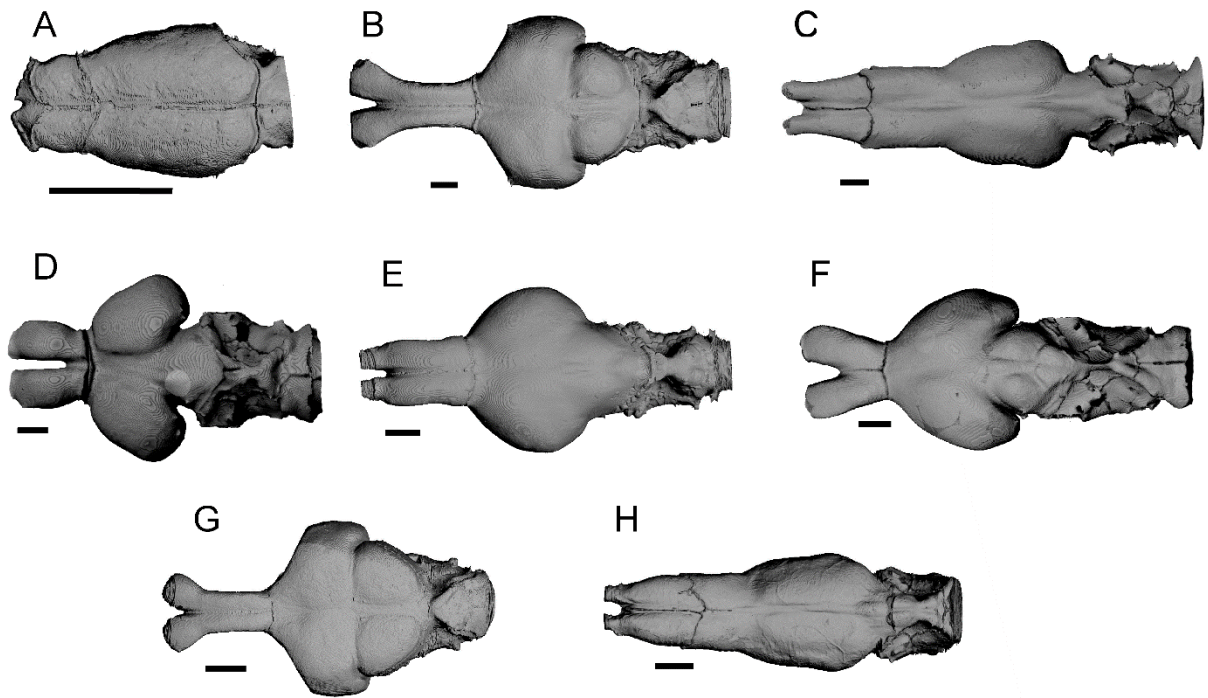
1084



1085

1086 **Fig. 3.** Skull of *Enhydris punctata* (Homalopsidae) in dorsal (A) and left lateral (B) views
 1087 showing the bones surrounding the brain endocast; (C-D) with bones rendered transparent to
 1088 reveal the brain endocast (green) and the inner ear (red). **Abbreviations:** **bo**, basioccipital; **bs**,
 1089 basisphenoid; **eo**, exoccipitals; **fr**, frontal; **p**, parietal; **pr**, prootics; **so**, supraoccipitals. Scale
 1090 bar equals 2 mm.

1091



1092

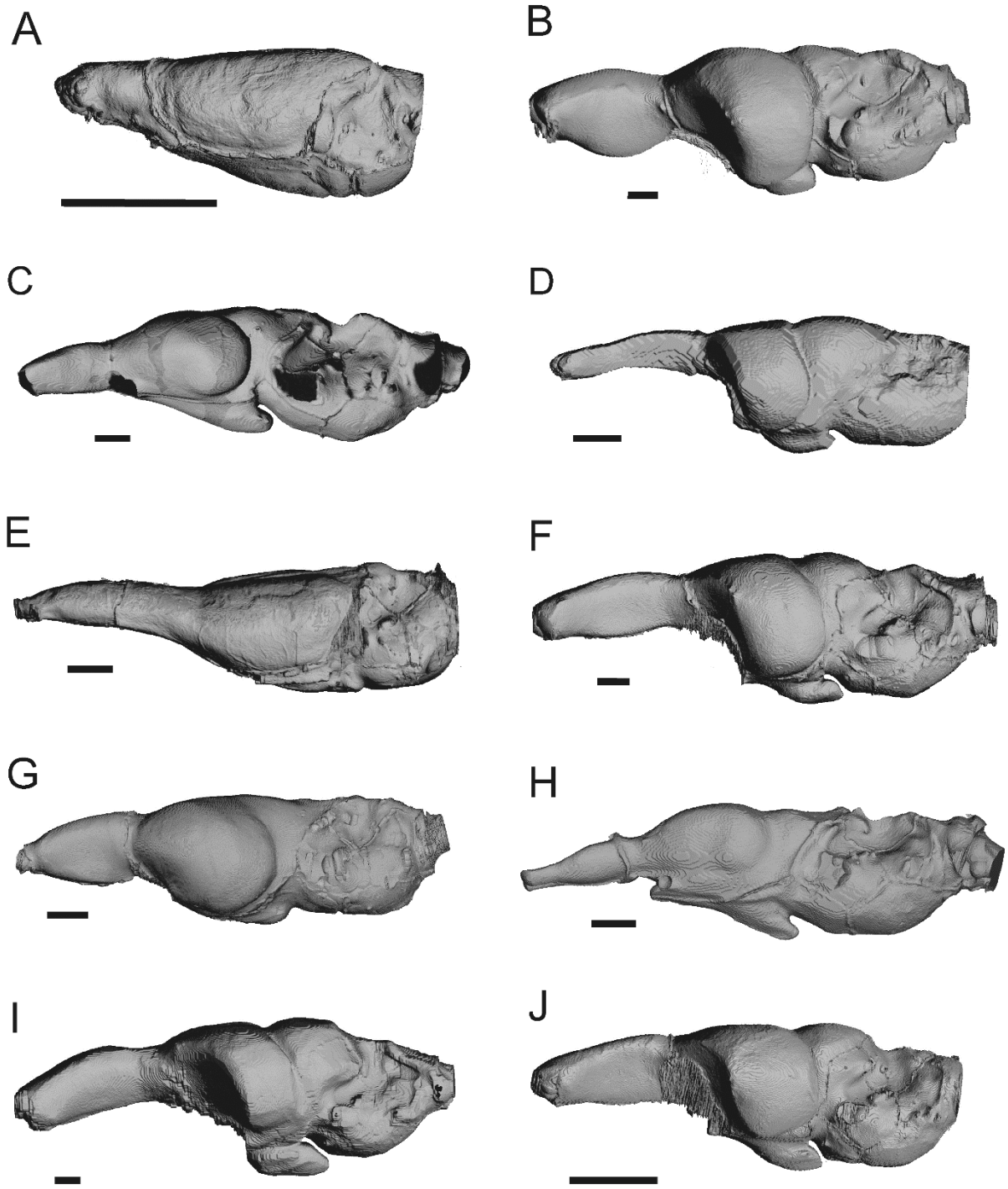
1093 **Fig. 4.** Brain endocasts in dorsal view of (A) *Typhlophys squamosus* (Typhlopidae); (B)

1094 *Hierophis viridiflavus* (Colubridae); (C) *Cylindrophis ruffus* (Cylindrophiidae); (D)

1095 *Acrochordus granulatus* (Acrochordidae); (E) *Eunectes murinus* (Boidae); (F) *Homalopsis*

1096 *buccata* (Homalopsidae); (G) *Chrysopelea ornata* (Colubridae); (H) *Anilius scytale*

1097 (Aniliidae). Scale bars equal 1mm.



1098

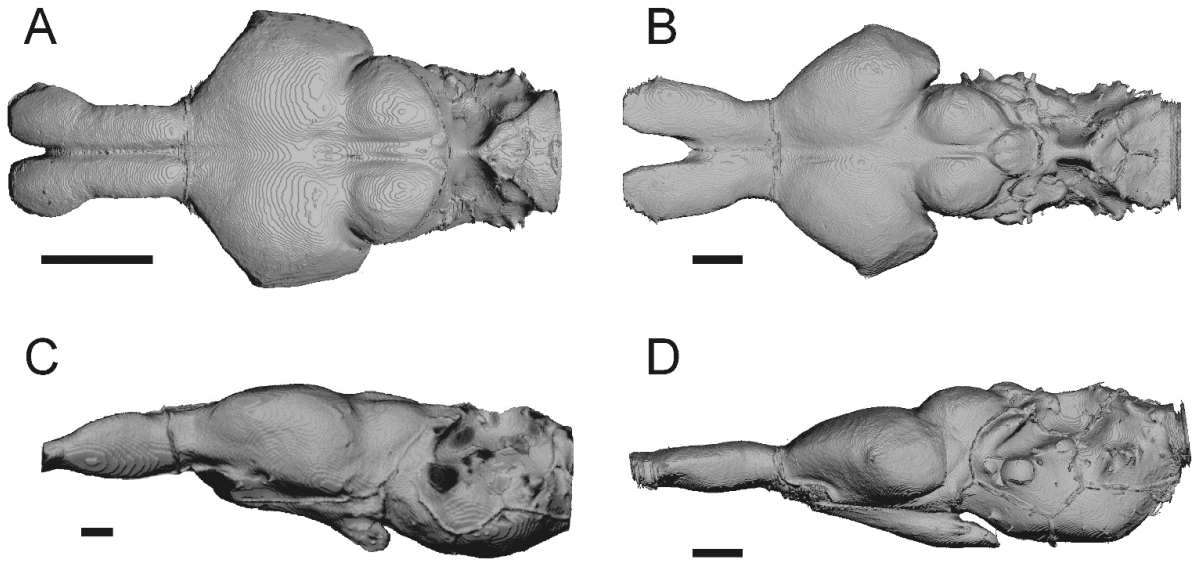
1099 **Fig. 5.** Brain endocasts in left lateral view of (A) *Typhlophys squamosus* (Typhlopidae); (B)

1100 *Boiga dendrophila* (Colubridae); (C) *Homalopsis buccata* (Homalopsidae); (D) *Mimophis*

1101 *mahfalensis* (Lamprophiidae); (E) *Anilius scytale* (Aniliidae); (F) *Hierophis viridiflavus*

1102 (Colubridae); (G) *Eunectes murinus* (Boidae); (H) *Enhydrina schistosa* (Elapidae); (I)

1103 *Dispholidus typus* (Colubridae); (J) *Thamnophis sirtalis* (Natricidae). Scale bars equal 1mm.



1104

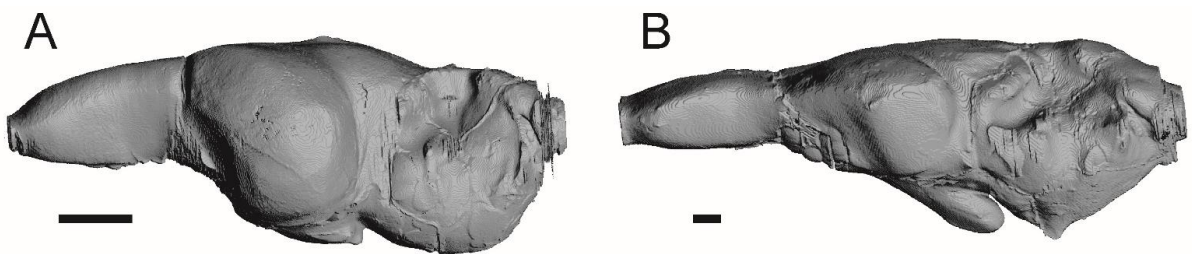
1105 **Fig. 6.** Brain endocasts in dorsal (upper row) and left lateral (lower row) views of (A)

1106 *Thamnophis sirtalis* (Natricidae); (B) *Erpeton tentaculatum* (Homalopsidae); (C) *Hydrophis*

1107 *major* (Elapidae); (D) *Erpeton tentaculatum*. Scale bars equal 1mm.

1108

1109



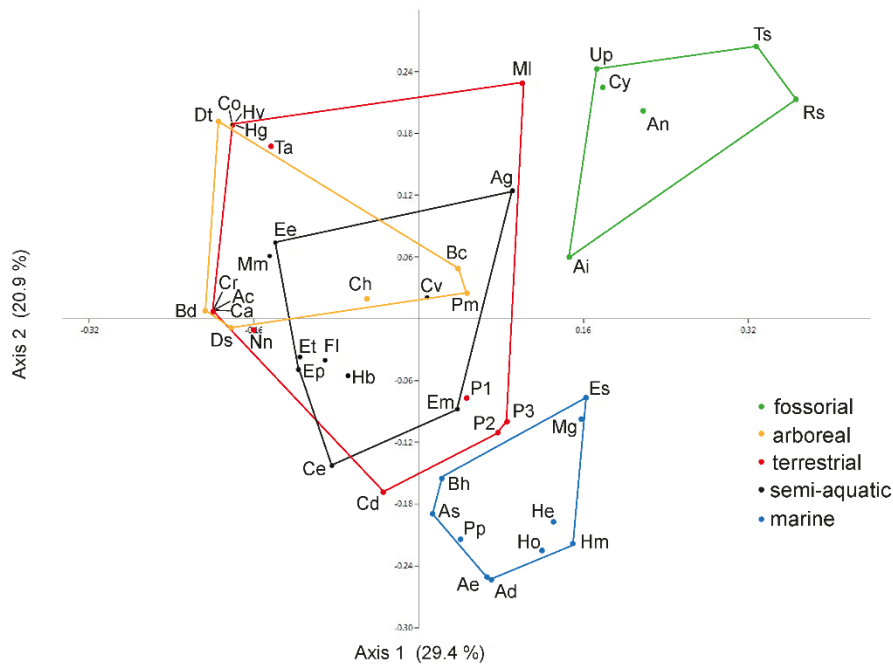
1110

1111 **Fig. 7.** Brain endocasts in left lateral view of (A) *Boa constrictor* (Boidae); (B) *Crotalus atrox*

1112 (*Viperidae*). Scale bars equal 1mm.

1113

1114



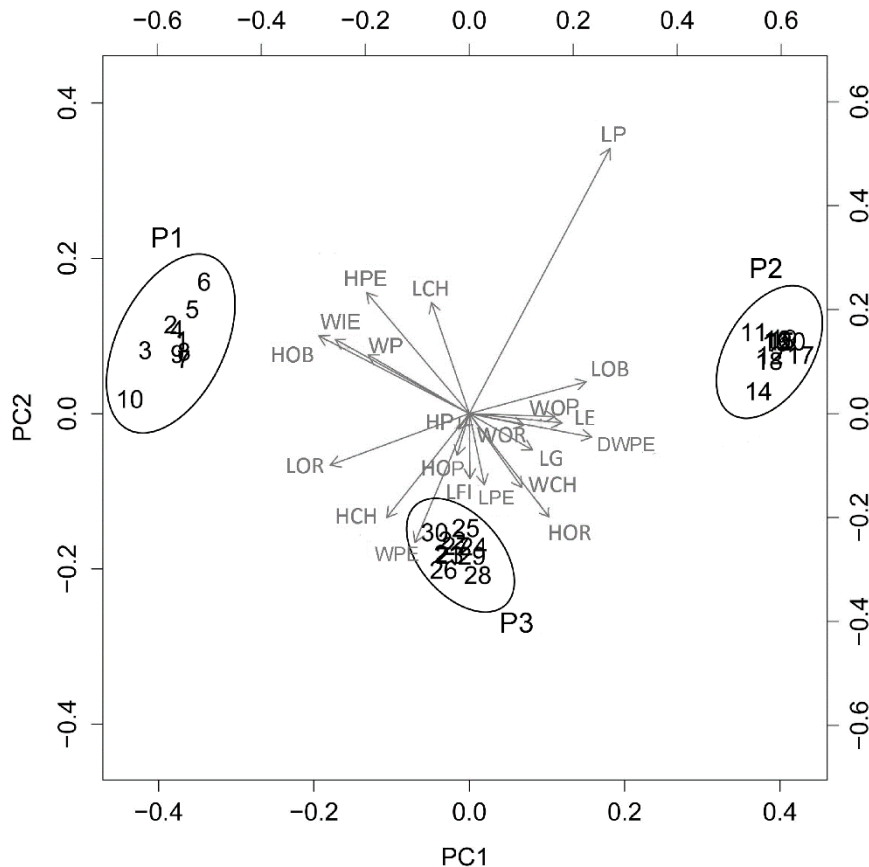
1115

1116 **Fig. 8.** Results of the principal coordinate analysis performed on the snake brain endocast

1117 characters (Supplementary Data S3). See Table 1 for name abbreviations.

1118

1119



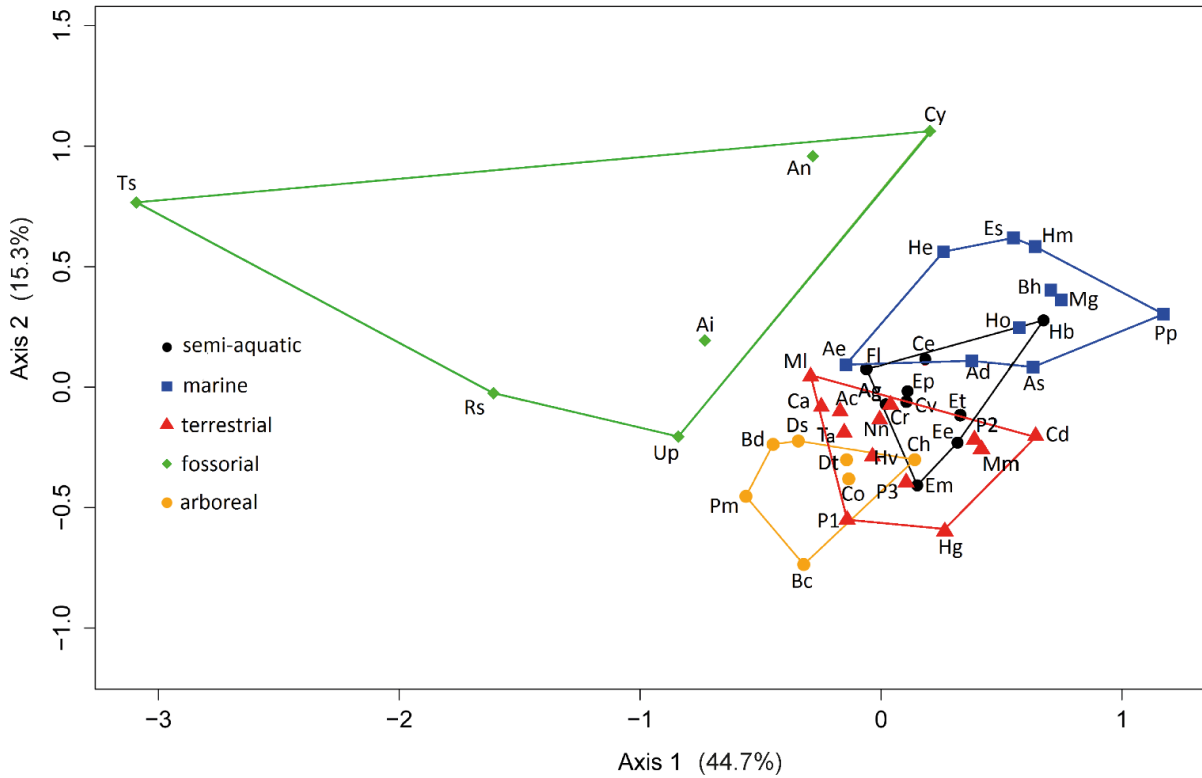
1120

1121 **Fig. 9.** Results of the principal component analysis performed on the brain endocast variables
 1122 for three *Python regius* specimens, (P1) smaller specimen, (P3) intermediate specimen, (P2)
 1123 largest specimen. Scatter plot illustrating the position of the different specimens on the first
 1124 two principal components. **Abbreviations:** DWPE, Dorsal width of the posterior end of the
 1125 brain endocast; HCH, Maximal height of the cerebral hemisphere; HOB, Height of the main
 1126 olfactory bulb; HOP, Height of the olfactory peduncle; HOR, Height of the optic tectum; HP,
 1127 Height of the pituitary bulb; HPE, Height of the posterior part of the brain endocast; LCH,
 1128 Lateral expansion of the cerebral hemispheres; LE, Length of the brain endocast; LFI, Length
 1129 of the interhemispheric fissure; LG, Length of the groove between olfactory bulbs; LOB,
 1130 Length of the olfactory bulbs; LOR, Length of the optic tectum; LP, Length of the pituitary
 1131 gland; LPE, Length of the posterior part of the brain endocast; WCH, Maximal width of the
 1132 cerebral hemispheres; WIE, Width in the inner ear region; WOP, Width of the olfactory

1133 peduncles; **WOR**, Maximal width of the optic tectum; **WP**, Width in the pituitary gland
 1134 region; **WPE**, Width of the ventral part of the brain endocast.

1135

1136

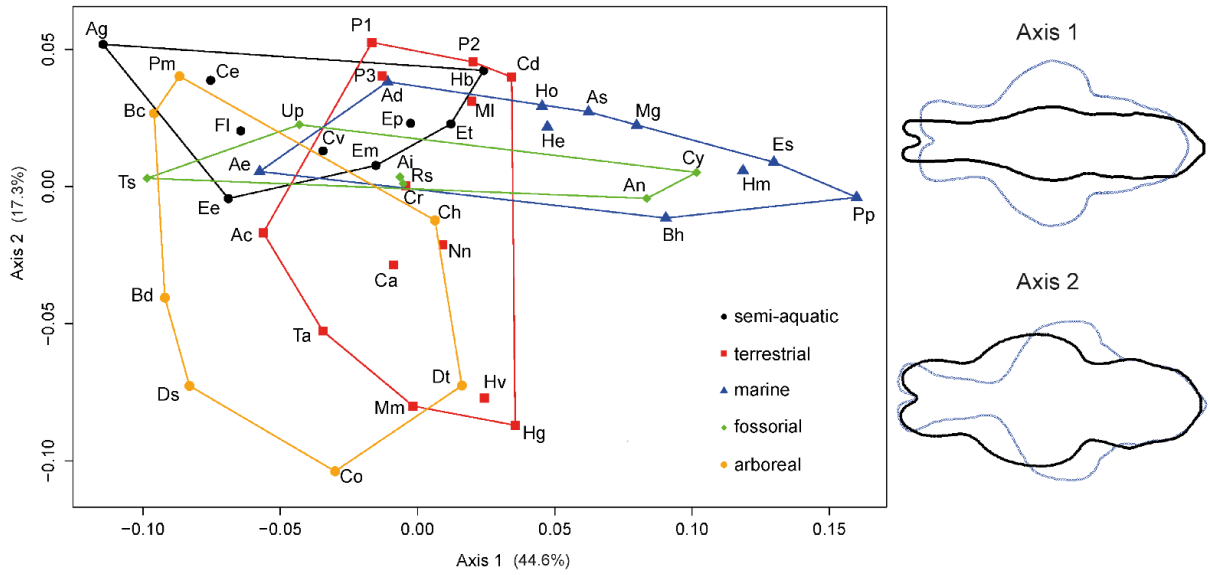


1137

1138 **Fig. 10.** Results of the principal component analyses performed on the snake brain endocast
 1139 variables of the 45 specimens. Scatter plot illustrating the position of the different species on
 1140 the first and second principal components and figuring the different ecologies. See Table 1 for
 1141 name abbreviations.

1142

1143

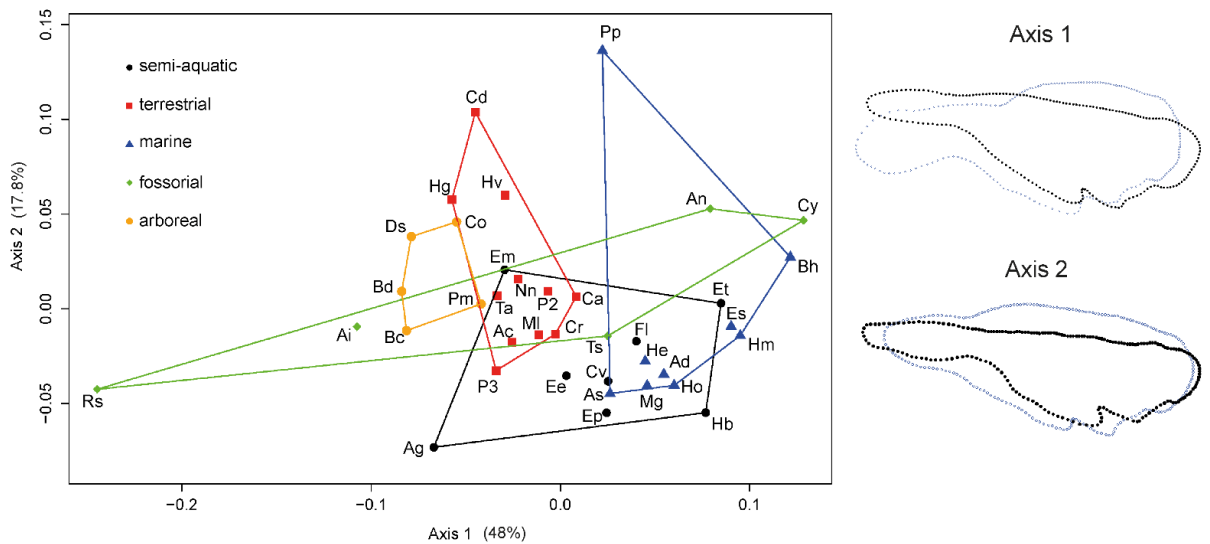


1144

1145 **Fig. 11.** Results of the principal component analyses performed on the snake brain endocast
 1146 outline curves in ventral view. The blue and dark dotted lines indicate respectively the low
 1147 and high values along the two axes. See Table 1 for name abbreviations.

1148

1149



1150

1151

1152 **Fig. 12.** Results of the principal component analyses performed on the snake brain endocast
 1153 outline curves in lateral view. The blue and dark dotted lines indicate respectively the low and
 1154 high values along the two axes. See Table 1 for name abbreviations.